A New One-Year Global Lagrangian Climatology of Mass Transport in the Lowermost Stratosphere

by

GEORGINA PAULL

Department of Atmospheric and Oceanic Sciences

McGill University
Montreal, Canada
November 2012

A thesis submitted to the Faculty of Graduate Studies and Research in partial fulfillment of the requirements for the degree of Master of Science

Acknowledgements

To begin, I would like to thank my supervisors, Professor Michel Bourqui and Professor David Straub. This thesis would not have been possible without their help and support. They helped my understanding of the subject as well as taught me how to write properly a scientific report (after many, many revisions). I would also like to thank the members of the stratospheric dynamics and chemistry group for their help and encouragement. Finally, none of this would have been possible without the help of Michael Havas, the computer guy, who fixed my computer countless times.

Abstract

We present the first year-long climatology of a new real-time global Lagrangian diagnostic system for stratosphere-troposphere exchange. This Environment Canada data set has been producing and archiving daily data since July 20th, 2010. A set of trajectories are calculated every day starting at 00:00 UTC using the operational global forecast. They are seeded every 5 hPa between 600 and 10 hPa over the entire globe with even horizontal spacing of 55 km. We examine the mass fluxes across i) the dynamical tropopause, which is taken to be the 2 PVU iso-surface, and ii) the 380K temperature surface. Pole-ward of approximately 20^o these two surfaces form a wedge called the Lowermost Stratosphere (LMS). The dynamics responsible for the transport across these two surfaces are very different. Mass flux across 380K, the upper surface, is driven by diabatic effects associated with the Brewer-Dobson circulation. Transport across the dynamical tropopause is dominated by quasi-isentropic mixing associated with baroclinic wave activity. The details of the transport across these two surfaces is known to determine the rate of injection of stratospheric ozone into the troposphere. This transport process is still today one of the major causes of uncertainty concerning the tropospheric ozone budget. Here we present the first one-year climatology of high-resolution global mass transport in the LMS, including geographical distributions and the Northern Hemispheric mass budgets, and will compare our results with previous studies.

Résumé

Nous présentons la première année de la climatologie en temps réel d'un nouveau système diagnostique lagrangien étudiant les échanges entre la stratosphère et la troposphère. Ce système d'acquisition, en fonction tous les jours à Environnement Canada, de données produit et archive quotidiennement les données depuis le 20 juillet 2010. Un ensemble de trajectoires est calculé chaque jour commençant à 00:00 UTC utilisant les prévisions météorologiques déterminées par Environnement Canada. Ils sont dispersées chaque 5 hPa entre 600 et 10 hPa également autour du globe avec un espacement horizontal de 55 km. Nous examinons le flux de masse i) entre la stratosphère et la troposphère, i.e. au travers de la tropopause dynamique (2 PVU iso-surface), et ii) à travers la surface à température de 380K. Dans les extra-tropiques, les deux surfaces se forment un region qu'on appele la haute troposphère et la basse stratosphère. Les dynamiques responsable pour le transport à travers ces deux surfaces sont très différentes. Le flux de masse à 380K, donc la surface supérieure, est déterminé par les effets diabatiques due à la circulation de Brewer-Dobson; alors que le transport à travers la tropopause dynamique est largement dominé par un mélange quasi-isentropique accompagné d'une activité de vagues baroclines. Les détails du transport entre ces deux surfaces sont connus pour déterminer le taux d'injection d'ozone stratosphérique dans la troposphère. Ce processus de transport est encore aujourd'hui une des causes majeures de l'incertitude concernant le budget de

l'ozone troposphérique. Dans cette thèse, nous présenterons la première d'une année en climatologie sur le transport de masse global entre la haute troposphère et la basse stratosphère, incluant les distributions géographiques et les budgets de masse de l'hémisphère nord, et nous comparerons nos résultats avec de précédentes études.

Contents

List of Figures

List of Tables

Chapter 1

Introduction

The phenomenon we call weather, and most of our lives, occurs in the troposphere, which is the bottommost layer of the atmosphere. Its name is derived from the Greek word ‘‘tropos’’, meaning to turn; this is fitting since the troposphere is characterized by vigorous overturning of air. In the tropics, this takes the form of convective clouds that can extend up to 20 km or more. This convection is fuelled by heating from below and can be thought of as forming a branch of the Hadley cells, which are thermally direct circulations that transport heat poleward from the tropics out to about 30^o latitude in both hemispheres. Tropical convection can also sometimes extend into the lower part of the stratosphere, where it connects to a meridional cell (Brewer-Dobson circulation) in the stratosphere. This cell is characterized by rising motion in the tropics, poleward flow in the extra-tropics, and sinking motion in the mid-latitudes. In the mid-latitudes, tropospheric convection is less vigorous. The troposphere is thinner and synoptic weather systems replace the Hadley cells as a means of transporting heat pole-ward.

Historically, studies of tropospheric and stratospheric phenomena were somewhat distinct; however, in recent decades it has become increasingly clear that exchanges between the two cannot be ignored. For example, exchanges of air parcels across the tropopause can not only affect the weather, but can also bring chemicals such as ozone from the stratosphere (where it is a useful absorber of harmful ultra-violet radiation) into the troposphere (where it is a pollutant). This thesis uses a new data set, which will be described in more detail in Chapter 2, to look at stratosphere-troposphere exchange by following air parcel trajectories as they move back and forth across the tropopause, i.e., across the boundary separating the two layers. This is the first one year climatology that studies the mass budget of these exchange events.

1.1 Vertical Temperature Profile

The Earth is surrounded by a thin layer of gases called the atmosphere. The most common way to separate the vertical structure is through its thermal characteristics. This gives rise to four distinct layers which are the thermosphere (which includes the exosphere and the ionosphere), mesosphere, stratosphere, and the troposphere as can be seen in Figure 1.1. The thermo-

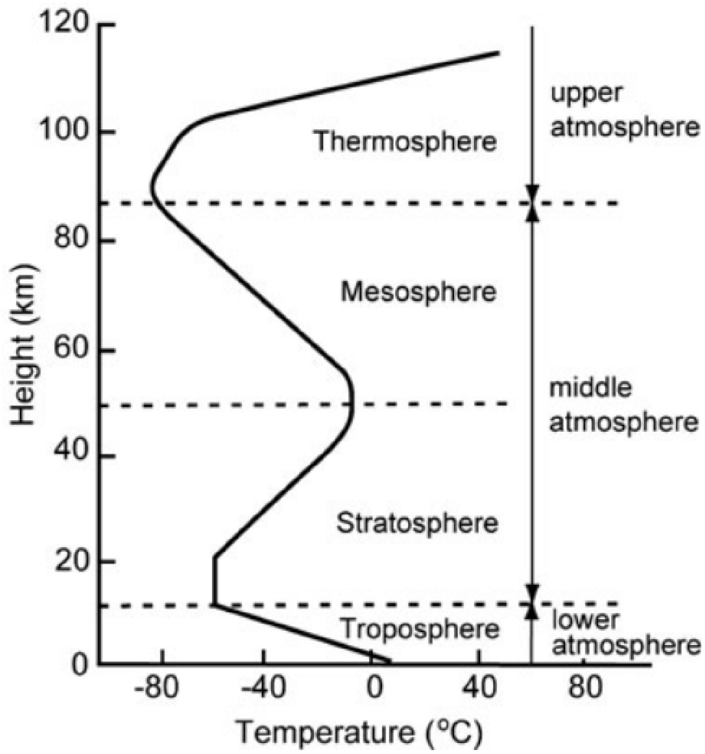

Figure 1.1: Thermal structure of the atmosphere

sphere is located around 100km in altitude and extends out to about 1300km, which is where outer space begins. Its temperature increases upwards and can become as high as 1300K. It is also within this layer that the atmosphere is ionized causing the reflection of radio waves. Below the thermosphere lies the mesosphere, with the two being separated by the mesopause at an altitude of about 80-90 km. The mesosphere is characterized by a decrease in temperature with height up to the mesopause which is the coldest part of the Earth's atmosphere dropping to as low as 130K.

Below the mesosphere lie the stratosphere and troposphere, which are the two layers of focus for this thesis. The stratosphere ranges from about 8-10km to about 50 km in altitude. This layer is characterized by an increase in temperature with height with a maximum around 270K. The stratosphere is layered in temperature due to the fact that in the uppermost part there is an abundance of ozone (O_3) which absorbs high energy ultra-violet radiation (UV) waves from the sun and is broken down into atomic oxygen (O) and diatomic oxygen (O_2). These two forms of oxygen then diffuse throughout the layer. Due to the fact that ozone is such an efficient absorber of UV, this allows the other two forms of oxygen to recombine into ozone in the mid-stratosphere. In this process heat is generated as a by-product. As a result of this vertical stratification (warmer temperatures over cooler ones) the stratosphere is dynamically stable with no thermally driven convection. Below the stratosphere lies the troposphere which is separated by the tropopause, located between 8-16 km depending on latitude and season. Temperature generally decreases with height within the troposphere and, at the equator, can vary between 300K at the surface to 200K at the top. At midlatitudes, there is less temperature variation because the troposphere is thinner. This part of the atmosphere holds approximately 80% of the mass as well as 99% of the water vapour and aerosols. The troposphere is characterized by a low concentration of ozone. In addition turbulent mixing plays an important role in the structure and dynamic behaviour of the troposphere specifically in the bottommost part (approximately 2km in altitude), called the planetary boundary layer, where friction can also affect the air flow.

1.2 Circulation and Mechanisms for STE Transport

1.2.1 Global Circulation

Hoskins [1991] distinguished between different regions of the lower stratosphere. He broke up the atmosphere into three separate regions called the "Overworld", "Middleworld", and "Underworld". The "Overworld" consists of those surfaces of constant potential temperature, also called isentropic surfaces, which lie above the tropopause (and generally lie above the 380K isentrope). Transport from this region to the troposphere is slow because air must undergo diabatic cooling or warming in order to cross a surface of constant potential temperature [Holton et al., 1995]. In the "Middleworld" isentropic surfaces cross the tropopause and the lowest isentropic surface grazes the Earth's surface. This allows for some isentropic surfaces to lie both in the troposphere and the lower stratosphere. Cross-isentropic transport is difficult, hence STE is favoured when isentropes extend from the stratosphere to the troposphere. This, typically, results in relatively fast transport between the lower stratosphere and upper troposphere and can occur in both directions [Chen, 1995]. Finally, the "Underworld" consists of all isentropic surfaces which lie completely in the troposphere.

The shaded region in Figure 1.2 represents the "lowermost stratosphere" which is also the stratospheric part of the "Middleworld" [Holton et al., 1995]. From hereafter we refer to this region as the Lowermost Stratosphere (LMS). In this thesis, the LMS includes the region of the atmosphere bounded above by the 380K isentrope and below by the dynamical tropopause, which is a surface of constant potential vorticity. It is within this region that mass can be exchanged with the troposphere along isentropic surfaces (wavy arrows in Fig 1.2) [Appenzeller et al., 1996]. Mass above the 380K isentrope can only be exchanged with the LMS by crossing isentropic surfaces.

Both upward and downward mass transport across the 380K isentrope is reasonably well understood and can be explained through our understanding of the stratospheric meridional circulation. This circulation was first inferred by Brewer [1949] and Dobson [1956] and is comprised of a single equator to pole cell which exists in the winter hemisphere where it reaches higher altitudes in the stratosphere. Air is lifted out of the tropical troposphere into the stratosphere. This tropical lifting is rather slow, on the order of 20-30 meters per day, which results in most of the air rising into the stratosphere never reaching the upper stratosphere. The air is then carried poleward where at around 30^oN and 30^oS the circulation becomes downward as well as poleward.

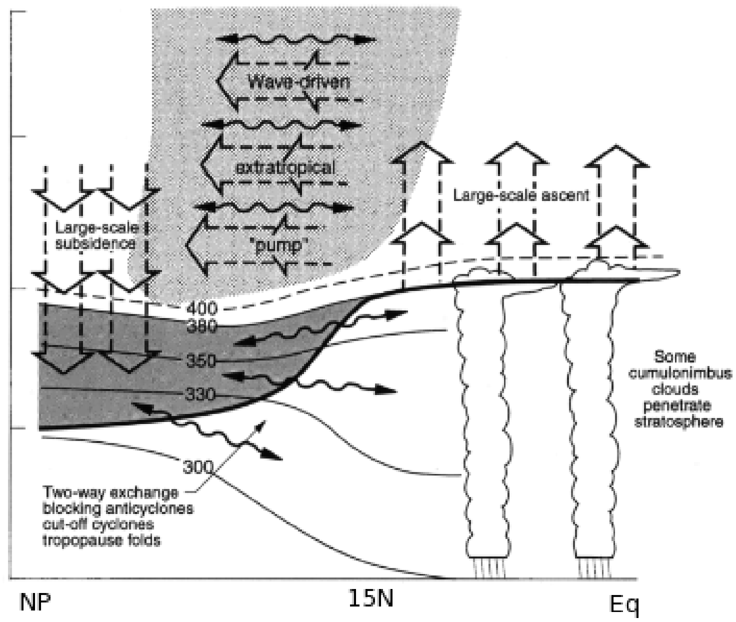

Figure 1.2: Dynamical aspects of STE in the framework of large-scale circulation. The thick black line is the dynamical tropopause, whereas the thin lines are surfaces of constant potential temperature [K]. The shaded region is the lowermost stratosphere. Taken and modified from Holton et al. [1995], their Figure 3.

This circulation, often referred to as the Brewer-Dobson circulation is driven by wave activity extending from the troposphere. Stationary planetary waves propagate vertically and as they break in the extra-tropical stratosphere, they deposit westward momentum. This can be thought of as a negative torque (in the opposite sense to the Earth's rotation) of air in the extra-tropical stratosphere. In response to this torque, air parcels migrate poleward so as to reduce the moment arm about the rotation axis. In other words this creates a “wave pump” which drives, to a large extent, the upper branch of the Brewer-Dobson circulation.

1.2.2 Mechanisms for STE Transport

Processes allowing mass transport across the upper and lower boundaries of the LMS differ. From the overworld, transport to the troposphere occurs slowly because the air must cross isentropic surfaces which requires diabatic cooling [Stohl et al., 2003]. Similarly from the underworld to the stratosphere diabatic warming is required which also makes the transport gradual. As described by Hoskins [1991], isentropic surfaces lie in the troposphere in the tropics as well as the LMS at higher latitudes. This results in quasi-adiabatic exchanges which leads to relatively fast transport across the dynamical tropopause which can occur in both directions [Chen, 1995].

Transport across the dynamical tropopause in the extra-tropics is associated with processes on length scales on the order of 10km-100km (mesoscale processes) and 100km-1000km (synoptic processes). It has been observed to occur in mesoscale convective complexes [Poulida et al., 1996], thunderstorms [Tremblay and Servranckx, 1993], due to the breaking of gravity waves [Lamarque et al., 1996], from events associated with baroclinic wave breaking events such as cut-off lows [Ebel et al., 1991, Wirth, 1995b], tropopause fold events around the polar jet [Danielsen, 1968] and the subtropical jet [Baray et al., 2000]. Tropopause folds and cut-off lows are of particular importance because they occur on a large scale resulting in the potential for larger exchange amounts of air.

Transport in the midlatitudes from the troposphere into the stratosphere has been observed less frequently. It is known that diabatic processes are important for this transport [Stohl et al., 2003]. Rapid transfer of tropospheric air into the lowermost stratosphere tend to be associated with areas of strong diabatic heating, such as by latent heat release from extratropical cyclones. Due to the relatively high stability of the lowermost stratosphere, air masses injected from the troposphere do not tend to reach high levels in the lower stratosphere, and especially not the stratospheric overworld [Stohl et al., 2003].

Mixing of air from the upper stratosphere to the lower stratosphere occurs on relatively larger time scales due to the fact that the air parcels must undergo diabatic heating or cooling in order to cross isentropes. On the other hand, transport from the lower stratosphere to the troposphere occurs quasi-adiabatically and thus is associated with shorter time scales.

1.3 The Tropopause

The tropopause is the boundary which separates the upper troposphere from the lower stratosphere. This surface is the lower boundary of the LMS as seen in Figure 1.2. It is a dynamical barrier which forces water vapour to remain mostly in the troposphere and ozone in the stratosphere. The definition and evolution of the tropopause concept has been largely driven by the available technology and scale of observations [Gettelman et al., 2011]. The different definitions of the tropopause are dependent on what a specific author is trying to research. If they wish to look at the chemical composition or the mass flux they would not use the same definition for both. This gives rise to three definitions; namely the chemical, thermal, and dynamical tropopause.

The chemical tropopause can be defined by using the gradient in concentrations of certain molecules. For example, the troposphere is characterized by a high concentration in water vapour and a low concentration in ozone whereas the stratosphere has a high concentration in ozone and a low concentration in water vapour. This result giving rise to a definition of the tropopause based on the difference of chemical composition between the layers. Bethan et al. [1996] defined the tropopause in terms of ozone concentration, by identifying the sharp gradient which occurs between the upper troposphere and the lower stratosphere.

The thermal tropopause is defined using a vertical temperature profile of the atmosphere. It is defined as the point where the air ceases to cool with increasing height. The thermal tropopause is defined as the lowest altitude where Γ, the environmental lapse rate, such that $\Gamma = \frac{\partial T}{\partial z} < 2$K/km, such that at any point at a vertical distance of 2 km above this point also has a $\Gamma <$ 2K/km [WMO, 1985]. This definition of the tropopause allows for multiple tropopauses, that are typically associated with folds, storms and stratospheric intrusions. This definition is often not ideal since it exhibits breaks near jet streams and does not form a continuous three-dimensional surface globally [Gettelman et al., 2011].

There is a need for a continuous global surface across which we can define the mass flux between the stratosphere and troposphere; therefore, using the previous definition is not ideal. This motivates the idea of using a dynamical quantity as the tropopause definition. The most commonly used variable is potential vorticity (PV). Most simply put, vorticity can be thought of as the tendency for elements of a fluid to spin. Mathematically, it is the curl of the three-dimensional velocity vector:

$$\vec{\omega} = \vec{\nabla} \times \vec{V} \tag{1.1}$$

The absolute vorticity, which is the sum of planetary vorticity and $\vec{\omega}$, of an air parcel will change if it is either stretched or compressed. However, if we assume this air mass to be bounded by two isentropes, surfaces of constant potential temperature, and there is no friction then we can divide the absolute vorticity by the vertical spacing between levels of potential temperature to create a conservative quantity called potential vorticity (PV) e.g. [Vallis, 2006]. Using Ertel [1942]'s definition, we define this as:

$$PV = \frac{(2\vec{\Omega} + \vec{\omega}) \cdot \nabla\theta}{\rho} \tag{1.2}$$

where ρ is the density of the fluid, $\nabla\theta$ is the gradient of the potential temperature, and $\vec{\Omega}$ is the planetary vorticity defined as:

$$\vec{\Omega} = \Omega(\hat{z} sin\theta + \hat{y} cos\theta) \tag{1.3}$$

where Ω is the angular frequency of the rotation of the earth (Ω=7.29x10^{-5}s^{-1})

Conservation of PV can be understood by an analogy with a spinning figure skater. When the skater has his arms out horizontally he will tend to spin slowly. Once he brings his arms in towards his body his speed of rotation increases due to the conservation of angular momentum. This same idea explains how air parcels react due to the conservation of PV. For example, assume that for a given parcel of air its PV is conserved and is thus bounded by two surfaces of constant potential temperature. If these isentropes stretch apart this will cause the $\nabla\theta$ term in Equation 1.2 to decrease. In order for PV to be conserved, and assuming constant air density, the absolute vorticity term must increase. This results in an increase in rotation of the air parcel. However, in order to conserve angular momentum, if the rotation of the air parcel increases its radius of rotation must decrease, analogously with the ice skater. This implies that a stretching of isentropes in the atmosphere will result in the convergence of air and the compression of isentropes leads to divergence.

The average potential vorticity, in the Northern Hemisphere, ranges approximately from 0.3 to 0.5 PVU[1] in the low and middle troposphere, and reaches 1 PVU in the upper troposphere. It then increases rapidly with height and takes on values much higher than 1 PVU in the stratosphere, due to the strong increase of the static stability. However, it is difficult to accurately choose one PV surface which best depicts the level of the tropopause since this value depends on both latitude and season. The value of PV is often chosen to correspond to the location of the thermal tropopause. Values ranging from 1.6 to 3.5 PVU are used throughout the literature (e.g. [Shapiro, 1980, Danielsen, 1968]); however, 2 PVU is observed to well represent the thermal tropopause [Holton et al., 1995]. It should be noted that using different PV tropopause definitions will result in quantitative differences in the calculated flux of stratosphere-troposphere exchange (STE) [Bourqui, 2006]. The sensitivity to this choice will be further discussed in Chapter 2.

All three of these definitions have their advantages and disadvantages. In this thesis, the PV-based tropopause is more appropriate because it acts as a quasi-material surface when looking at stratosphere-troposphere exchange in the middle latitudes [Hoskins et al., 1985]. The PV definition of the tropopause provides a dynamically consistent framework for estimating STE. This is crucial since it is this framework which allows us to study the transport across the tropopause.

[1] 1 PVU= 10^{-6} Km^2 kg^{-1} s^{-1}

1.4 Methodologies for Estimating STE Flux

In order to diagnose fluxes across the tropopause, the method used must be capable of resolving motions of the flow and the tropopause at the scales on which the physical processes are acting [Bourqui, 2006]. In addition to this, these methods must be applicable to global meteorological data in order to produce global scale estimates. Before selecting the most appropriate method, we compare and contrast four different methodologies used in previous studies:

1. Methods based upon Eulerian formulations of the cross-tropopause flux and estimating individual terms of the formulation

2. Methods explicitly estimating the non-advective part of the motion of the tropopause

3. Methods using a trajectory-based Lagrangian representation of the flow (i.e. Methods which follow the flow of a trajectory)

4. Methods using transport schemes with physics parameterizations and estimating the cross-tropopause transport of a tracer

The study of Wirth and Egger [1999] inter-compared three different methods based upon Eulerian formulations, a method of Type_1, a method of Type_2, and a trajectory-based Lagrangian method, Type_3. The methods were compared to a case study of an episode of a cut-off cyclone. A data set was obtained from a run of the European Centre for Medium-Range Weather

Forecast model. When comparing the different Eulerian methods, Type$_1$, they produced reasonable results when PV was used as a vertical coordinate. They noted that in many practical applications the PV field is not given as part of the data set thus requiring the use of either θ or pressure as the vertical component. When θ or pressure was used for the Eulerian based method, Type$_1$, their results revealed that in both the upward and downward direction there was a large amount of cross-tropopause flux due to numerical noise [Wirth and Egger, 1999].

Analysis of Type$_2$, also known as the direct method, had similar issues as the two Eulerian based methods of Type$_1$. However the direct method, Type$_2$, provided insight as to the origin of the problems. They suggested that the difficulties with the mass flux calculation most likely arose from the insufficient accuracy and consistency of the data.

Of the three different Eulerian methods and the direct method, the only reasonable estimate for both upward and downward mass flux came from using PV. However, this method of Type$_1$ is not always ideal because in many applications, the PV field is unavailable and must be indirectly computed from the available data. This may give rise to a deterioration of the results which removes the advantage of using this method over the others.

Wirth and Egger [1999] also implemented a method of Type$_3$. This trajectory based method was found to be as successful as the Eulerian method when using PV as the vertical component. However, the Lagrangian based method is advantageous because it does not require the knowledge of the non-conservative fields [Wirth and Egger, 1999]. On the other hand, it is computationally expensive. In a similar inter-comparison study, Kowol-Santen et al. [2000] compared exchange events of $Type_1$, using PV as the vertical component, and $Type_3$. They found there was close agreement when looking at the net mass flux, but that $Type_1$ was much noisier when broken up into the individual up and down flux components [Kowol-Santen et al., 2000].

Gray [2003] used a mesoscale model to derive the fluxes of stratospheric air through the tropopause using a passive tracer, $Type_4$. Her results were very sensitive to horizontal and vertical resolution as well as the diffusion coefficient. It was also shown that a large portion of the cross-tropopause mass flux came from the model's explicit advection and from parameterized turbulent mixing. The advantage of using this method over the others is that it allows for isolation of the contribution of individual processes. This method, however, does not provide direct information either on the timescale or on the spatial distribution of exchange, and results tend to be noisier [Gray, 2006].

For the following project, the Lagrangian based method, $Type_3$, was chosen over the others for two reasons. First, it can resolve individual exchange processes when looking at net STE, stratosphere-to-troposphere transport (STT), and troposphere-to-stratosphere transport (TST) whereas the other methods are either incapable, or do so inaccurately. Second, only the Lagrangian approach is capable of considering both intrusion depths and residence times in order to characterize relative importance to given exchange events [Gettelman et al., 2011].

The approach used for this project is based on the adapted Lagrangian version, Type_3, introduced by Wernli and Bourqui [2002]. This method uses trajectories which are initiated on a three-dimensional grid and then computed using winds from an operational analysis data set [Wernli and Bourqui, 2002]. Exchange events were selected if a trajectory had a threshold residence time, τ^*, of 12h on either side of the cross-tropopause point. This idea was implemented to select significant exchange events. They suggested that possible errors due to trajectory calculation as well as the calculation of PV would likely introduce spurious exchange events with short residence times. A study performed by Stohl et al. [2003] found that this trajectory-based Lagrangian method accurately identified regions of exchange events and provided realistic quantitative lower bound estimates.

1.5 Spatial Patterns and Seasonal Variability of STE

1.5.1 Stratosphere-to-Troposphere Transport

When looking at Lagrangian climatologies of exchange events across the 2 PVU surface [James et al., 2003, Sprenger and Wernli, 2003], spatial patterns for upward and downward transport differ. Both climatologies show an abundance of downward transport across dynamical tropopause (2 PVU) in the extratropical regions. This is due to the fact that the preferred regions for transport occur near baroclinic instabilities. In the Northern Hemisphere, these regions are associated with the Atlantic and Pacific storm track and often over the Mediterranean. However, STT, or downward transport, varies both in magnitude and position depending on the season.

The spatial pattern over the winter (December, January, February) tends to be concentrated over the Pacific and Atlantic oceans. During the summer season (June, July, August), the storm track patterns are weaker, thus there is a general shift of STT over the continents. Some regions of enhanced STT, such as over Turkey and Kazakstan, correspond to particularly strong bands of upper tropospheric baroclinicity which is possibly a result of tropopause folding as the driving exchange process for these regions [Sprenger and Wernli, 2003].

1.5.2 Troposphere-to-Stratosphere transport

Troposphere-to-stratosphere transport (TST), upward transport, does not tend to vary either spatially or seasonally as much as STT. These events tend to be concentrated near the poles as opposed to the extra-tropical regions. Spatially the pattern is smoother, however, there are some regions of preferred transport. Such areas of strong diabatic heating located near the east coast of Asia and North America, especially during the winter, are some examples [Sprenger and Wernli, 2003].

The winter season tends to have slightly increased frequency and magnitude when compared with the summer season. There is one exception, this is the summer maximum located over the eastern Mediterranean. This area of enhanced TST was explained by Sprenger et al. [2003] who carried out a global investigation of tropopause fold events. This region over the Mediterranean coincides with a preferred area of summertime tropopause folding associated with the entrance region of the Asian jet stream which marks the northern edge of the large-scale monsoon anticyclone [Gettelman et al., 2011]. A more in depth look into the spatial patterns of both TST and STT will be carried out in Chapter 3.

1.6 Motivations and Goals of this Thesis

The exchange of air mass between the troposphere and stratosphere has important implications. Injection of ozone rich stratospheric air into the planetary boundary layer enhances low level O_3 concentration. This acts to alter the chemical composition in the lower troposphere as well as the radiation budget [Bourqui and Trépanier, 2010]. In addition, recent studies have suggested that cross-tropopause flux may increase over the present century as a result of climate change [Sudo et al., 2003, Collins et al., 2003]. Thus, it is important to understand further the dynamics of the mass flux across both the 380K isotherm and the dynamical tropopause (i.e., the mass flux into and out of the LMS). Using this new data set, the goals for this thesis are the following:

1. To explore and evaluate the first one year climatology of this new data set such that it can be used for further research and understanding of stratosphere-troposphere exchange

2. To analyze the mass budget of the lowermost stratosphere (LMS)

3. To study the relationship between the transport across the tropopause and the Brewer-Dobson circulation in the lower stratosphere

Our main goal is to explore the new data set using a Lagrangian based methodology and the Global Environmental Multi-scale (GEM) operational forecast in such a way that it can be used in further studies. This is the first data set in which forecast data is used to calculate the movement of trajectories as well as the mass flux across the tropopause on a climatological scale. An emphasis was placed on the mass flux across the 380K isentrope and the dynamical tropopause because these are the upper and lower boundaries, respectively, of the LMS. The specific details of the data set are outlined in Chapter 2 and the results in Chapters 3 and 4.

Chapter 2

Methodology

This thesis is based upon a data set which was initiated in July 2010. It follows the same methodology outlined by Bourqui [2006] applied globally, and will be described in further detail in the following section. This is the first study to be based solely upon forecast data and to provide global estimates of STE using the Lagrangian method.

2.1 Description of Data Set

The cross-tropopause mass flux calculation is based on the output data from the Global Environmental Multi-scale (GEM) numerical weather prediction model which provides hourly meteorological fields with horizontal grid spacing of 0.3°x0.3° and 80 hybrid levels up to 0.1 hPa. Trajectories are then computed using an adapted version of the LAGRangian ANalysis TOol (LAGRANTO) proposed by Wernli and Davies [1997] which is based upon a Eulerian iterative scheme.

A set of 15 million trajectories are globally initiated with even horizontal spacing of 0.5° and vertically every 5 hPa between 600hPa and 10 hPa. They are initialized at time t=0h of the forecast and ran for up to 6 days. In order to calculate the mass fluxes, we selected trajectories which crossed either boundary of the lowermost stratosphere over a 24h window. More specifically a trajectory is selected if it fulfills the following:

1. It must cross either the 2 PVU or 380K iso-surfaces within the time window [12h,36h]

2. It must have a residence time of at least 12h on either side of the cross-tropopause point

The threshold residence criterion is imposed in order to remove spurious oscillations around the tropopause caused by numerical noise [Bourqui, 2006]. An example of a selected trajectory can be seen in Figure 2.1.

These two criteria reduce the number of trajectories by a factor of 100, from 15 million to approximately 150 000 [Bourqui et al., 2012]. The three-dimensional position coordinates, along with potential vorticity and potential temperature values are archived every hour along the selected trajectories. The trajectories from each day were grouped together to form a

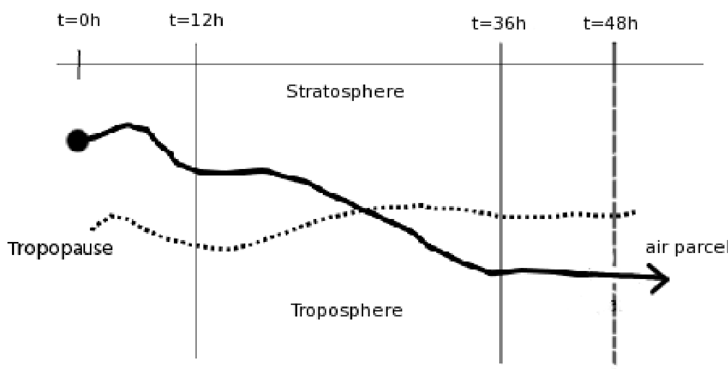

Figure 2.1: Example of a selected trajectory passing down through the tropopause initiated at time t=0h of the forecast.

one year climatology of STE events spanning from September 2010 to August 2011. From the same forecast, a new set of trajectories is started at 24, 48, 72, and 96 UTC. The same selection criteria is followed representing STE within the time windows [36h, 60h], [60h, 84h], [84h, 108h] and [108h, 132h] respectively. Similarily, these trajectoires were grouped together to make four more one year climatologies based on forecast time. An example of how the five climatologies were created based on forecast time can be see in Figure 2.2. All of the trajectories for this year which crossed the first time window (red) were grouped together, all of those which crossed the second (blue) were grouped together and so forth.

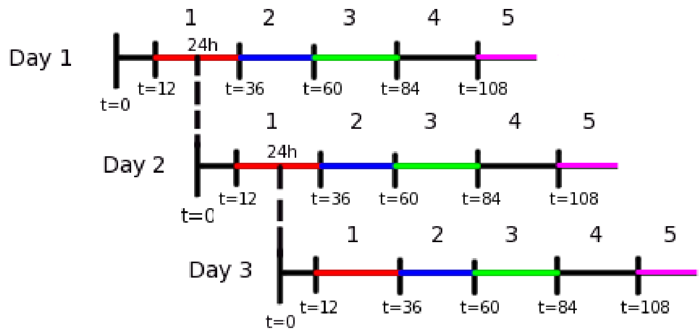

Figure 2.2: Example of how the five yearly climatologies were created. The red line corresponds to the trajectories which crossed the first time window, the blue line the second forecast time window, the green line the third forecast time window, the black line the fourth forecast time window, and the magenta the fifth forecast time window.

From these trajectory calculations, global geographical mass flux maps were created. There were four different maps, these being the maps associated with transport both upwards and downwards across both the 380K isentrope and the 2 PVU iso-surface. For this thesis, the depth to which a trajectory penetrates into the stratosphere or troposphere was ignored. Note that not all trajectories selected by the above criteria correspond to parcels entering or leaving the LMS. This is typically the case of a trajectory crossing at high latitudes as can be seen in Figure 1.2 but not always the case for trajectories in the tropics. For this reason, the following filtering was applied for the Northern Hemisphere:

1. If a trajectory crossed the 2 PVU iso-surface, either up or down, it must have a potential temperature less than 380K
2. If a trajectory crosses the 380K isotherm, either up or down, it must have a potential vorticity larger than 2 PVU

Note that when a crossing event occurred, its potential temperature or vorticity at that moment was calculated using linear interpolation between the previous time step and the following one.

For convenience, and to allow for comparison with the literature, the units of the mass flux density maps were rescaled to kg $km^{-2}s^{-1}$. From Bourqui [2006], the mass associated with each trajectory is approximately 157x10^9 kg. The distance corresponding to 2° latitudinally is constant at approximately 222 km. However the longitudinal distance for 2° varies from the equator to the pole. The length of a degree of longitude depends only on the radius of the latitude circle. If we assume the Earth to be a sphere of radius R (where R=6378.1 km) then the radius of a circle at latitude ϕ would be R$\cos\phi$. Equation 2.1 then demonstrates how to calculate 2° of longitude based on the latitude ϕ.

$$d(km) = \frac{2\pi * 6378.1}{180} \cos(\phi) \tag{2.1}$$

2.1.1 Calculation of Mass Flux

This thesis is based on mass exchange between the stratosphere and troposphere. Specifically, we studied the transport across the dynamical tropopause (2 PVU surface) and the 380K isentrope. It is, therefore, important to understand how the mass flux is calculated. Mass flux across a surface is defined as:

$$F(\rho) = -\int_{2} \frac{\rho}{|\nabla Q|} \frac{\mathrm{dQ}}{\mathrm{d}t} d\sigma \tag{2.2}$$

Where ρ is the density, Q is the potential vorticity, and dσ along with the subscript on the integral denote the surface area of the chosen layer to calculate the mass flux across. For example, the above formula calculates the mass flux across the 2 PVU tropopause (positive downwards) [Bourqui, 2001].

2.2 Sensitivity of the Methodology

Both the magnitude and spatial pattern of these cross-tropopause fluxes are sensitive to factors such as threshold residence time, data resolution, and PV tropopause definition. In order to accurately calculate cross-tropopause exchange events, it is necessary to understand how each factor affects the trajectories. For example, the use of data resolution which is too coarse may miss some exchange events and lead to an inaccurate representation of cross-tropopause mass flux. Bourqui [2006] provided a sensitivity analysis of how these factors affect STE events which will be further discussed in the following section.

2.2.1 Threshold Residence Time

The calculation of PV from finite resolution data and the calculation of the trajectories can create numerical errors [Bourqui, 2006]. These numerical errors may result in high frequency oscillations around the tropopause. This results, for example, in an air parcel moving downwards across the tropopause only to return upward shortly thereafter. James et al. [2003] found that 90% of the cross-tropopause flow returned to its original layer within 6 h, which supports the notion that the distinction between short and long residence times is crucial. This led to the idea of imposing a minimum threshold residence time, τ^*, which is a constraint that requires a trajectory to remain on either side of the cross-tropopause point for a certain amount of time. This acts to filter out high frequency oscillations which are not considered significant exchange events.

A study performed by Bourqui [2006] compared how different minimum threshold residence times influence stratosphere to troposphere transport (STT), troposphere to stratosphere transport (TST), and the net exchange when looking at a baroclinic wave breaking event. Their results showed that for $\tau^* = 0$h the individual fluxes in the upward and downward directions were three to five times larger than that when τ^* =12h. Additionally, the temporal evolution was significantly different. For the net (STT-TST) mass flux across the 2 PVU surface, their results yielded similar values for the two threshold residence times. This supports the results of James et al. [2003], that a large number of the exchange events have residence times less than 12h and cancel each other at each time step in the net flux. Bourqui [2006] also compared minimum threshold residence times of 12, 24, 36, and 48h. The results showed that the most significant differences between the residence times was the total magnitude of the mass flux. As the time constraint increased the magnitude of upward and downward flux decreased. The increase in τ^* had no effect on the temporal evolution of the mass flux and the net exchanges were comparable for all residence times.

2.2.2 Data Resolution

Processes such as thunderstorms are known to be triggering mechanisms for stratosphere troposphere exchange events. In order to calculate accurately the mass flux the resolution must be fine enough such that it captures these small scale events, yet remain coarse enough so that it is not too computationally expensive. In a sensitivity analysis performed by Bourqui [2006] they studied how degrading the spatial and temporal evolution affects cross-tropopause mass flux. They found that degrading the spatial resolution from 0.5^o to

1^o produced similar results. Further reducing the resolution to 2^o, however, produced severe under-estimates of downward transport during the break-up and decay phase of a baroclinic wave breaking event. On the other hand, upward transport did not show a clear response to the degradation of the spatial resolution. There was, however, a significant difference in the temporal structure for the coarsest spatial resolution. Both downward and upward transport were slightly overestimated when going from 1h to 3h resolution [Bourqui, 2006]. It is evident when calculating the mass flux between the stratosphere and troposphere the choice of spatial and temporal resolution size is essential.

2.2.3 Dependence on PV Tropopause Definition

Both the magnitude and temporal evolution of STE events are sensitive to the chosen value of potential vorticity (PV) for the dynamical tropopause. As one might expect, the total magnitude of upward and downward mass flux decreases as the PV level increases. The temporal evolution, however, of the mass flux is sensitive to changing tropopause levels. This can be seen in the study of Bourqui [2006] who examined the evolution of a baroclinic wave breaking event. It was concluded that the maximum magnitude of mass flux decreased as the PV value of the dynamical tropopause increased. The only surfaces which showed an increase in magnitude of the exchange events occurred between 1.5 and 2 PVU. This suggests that the use of 2 PVU as the value for the dynamical tropopause may accurately represent the transition between the stratosphere and troposphere.

In summary, when calculating the mass flux between the stratosphere and troposphere, it is evident that the choice of the dynamical tropopause, the minimum threshold residence time used, and both the spatial and temporal resolution affect the amount of transport. The use of the 2 PVU surface is often chosen because it reasonably approximates the thermal tropopause in the extra-tropics [Holton et al., 1995]. In order to capture all of the events which affect STE events, it is necessary to use high resolution data, i.e. 0.5^o and 1h. The use of a minimum threshold time is required to filter out spurious oscillations of trajectories around the tropopause. It has been shown that the use of $\tau^* = 12$h produces a nearly unbiased representation of stratospheric intrusions [Bourqui et al., 2012].

Chapter 3

Comparison of STE with Previous Studies

There have been many previous studies that have used the Lagrangian trajectory approach to examine stratosphere troposphere exchange [Sprenger and Wernli, 2003, Wernli and Bourqui, 2002]. This is the first attempt at using an operational forecast model to initiate and calculate trajectories on a climatological scale. For this reason, it is necessary to compare the initial results with previous studies to evaluate the accuracy and potential of using this technique for future studies. When studying cross-tropopause mass flux it is important to look at both the spatial pattern as well as the total magnitude of the exchange events. In a first step, we compared our initial results to results from the Sprenger and Wernli [2003] study.

The Sprenger and Wernli [2003] study was chosen for comparison because of its similarities with our work. They used the European Centre for Medium-Range Weather Forecasts (ECMWF) reanalysis data (ERA 15) spanning 15 years from January 1979 to December 1993. Similarly to Wernli and Bourqui [2002], they initiated their trajectories every 24 hours on a regular grid with a horizontal spacing of 80 km and vertically every 30 hPa between 590 hPa and 80 hPa. They also used the Lagrangian methodology first introduced by Wernli and Bourqui [2002], as well as using the 2 PVU definition for the tropopause in the Northern Hemisphere extra-tropics. There are two noteworthy differences, the first being that they used a minimum threshold residence time, τ^*, of 96 hours whereas we used 12 hours. With this difference, we would not expect a difference in the location of exchange events over the Northern Hemisphere. On the other hand, we would expect our data set, with the residence time of 12 hours, to have larger number of events per specific location. The second difference is the horizontal resolution of the two data sets. Their resolution was coarser, 2^o x 2^o, as oppose to ours, 0.5^o x 0.5^o. This may result in their study missing some events, such as those associated with thunderstorms, because the resolution is too coarse. Note also that their paper only looked at the mass flux across the 2 PVU surface which, in our case, is the bottommost layer of the lowermost stratosphere. Unfortunately a similar data set is not available for validation of our calculations across the 380K isentrope.

Initially, we compared the magnitude and spatial patterns of the exchange

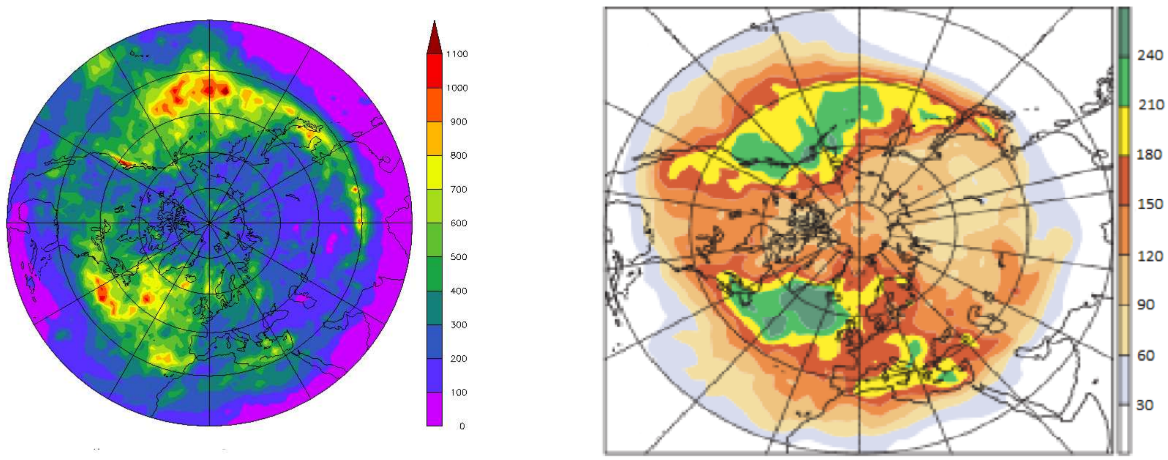

Figure 3.1: Comparison of downward mass flux (STT) across the 2 PVU iso-surface between our results (left) and the result from Sprenger and Wernli [2003] (right) for the Northern Hemispheric winter (DJF). Both results are in $\mathrm{kgkm^{-2}s^{-1}}$

events across the dynamical tropopause by looking at the mass flux density maps. Figure 3.1 compares the downward mass flux across the 2 PVU surface with analogous results from their study. During the winter, which is taken to be December, January, and February, we see a close resemblance between the two data sets. Both show maxima over the Pacific and Atlantic storm tracks, which correspond to regions of high baroclinic wave activity.

In general, the signal over the continents is much weaker. There are a few regions of discrepancy over the continental region between the two data sets. One of which is found along the southwestern coast of North America. The maximum over the Pacific storm track in Sprenger and Wernli [2003] continues further into the western coast of North America than we see in our results. There is one notable difference over the Mediterranean region; our results show less activity compared to the Sprenger and Wernli [2003] study; these differences will be discussed in Chapter 5.

Figure 3.2 compares the spatial patterns of STT during the summer season, June, July, and August. Due to the fact that storm track patterns are weaker in the summer, there is a shift of events onto the continents. In general, there are a lot of similarities between the two results with respect to STT in the summer and winter season. There do exist some slight differences

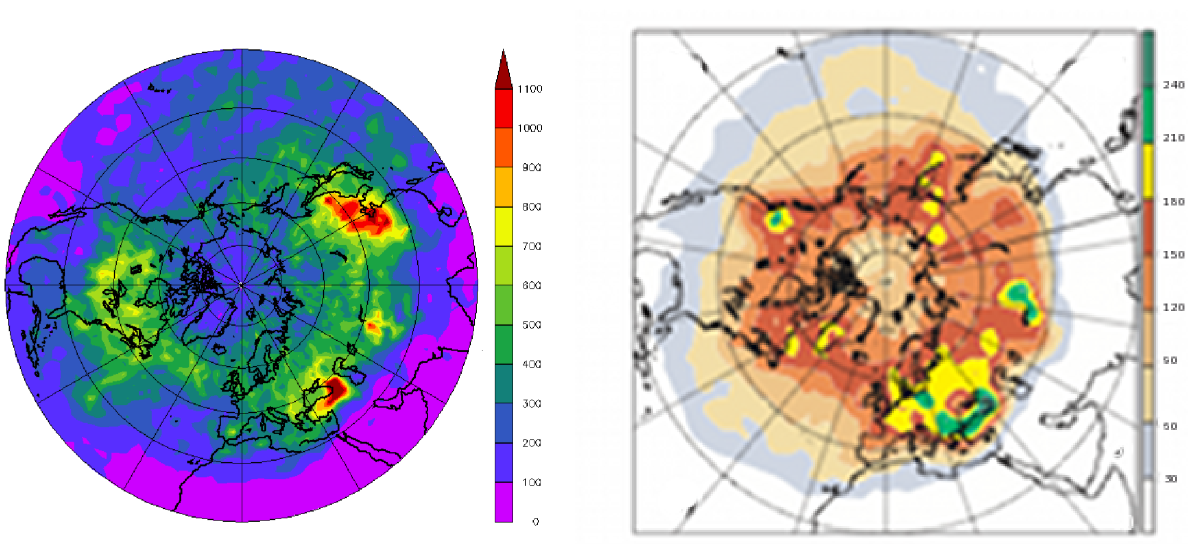

Figure 3.2: Comparison of downward mass flux (STT) across the 2 PVU iso-surface between our results (left) and the result from Sprenger and Wernli [2003] (right) for the Northern Hemispheric summer (JJA). Both results are in kgkm^{-2}s^{-1}

over North America as well as a large discrepancy over Eastern Asia. Looking at the western Canadian coastline, our results show a minimum whereas Sprenger and Wernli [2003] have a maximum. A similar difference occurs over the Great Lake region where our results show a weak maximum and their results show a minimum. There is also another discrepancy over Eastern Asia, where our results show a strong maximum and theirs have significantly less activity. One possible explanation for this difference is from exchanges associated with the Asian monsoon. This hypothesis and other explanations will be discussed further in Chapter 5.

Figures 3.1 and 3.2 show clear regions of preferred downward flux from the stratosphere to the troposphere. As was previously mentioned in Chapter 1, this is not the case when looking at upward transport across the dynamical tropopause. Instead of there being a few regions of intense transport, there is a smoother spatial pattern across the Northern Hemisphere. This can be seen in Figure 3.3 which compares the upward exchange events across the 2 PVU surface (TST) from our study with that from Sprenger and Wernli [2003]. Note only the winter season for TST is shown; the summer season has a similar spatial pattern, but with a weaker signal. It can be seen that there is a general shift of TST towards higher latitudes when comparing with STT. The spatial pattern is also smoother and has weaker maxima then when looking at STT.

To summarize, although there are some differences, in general our results

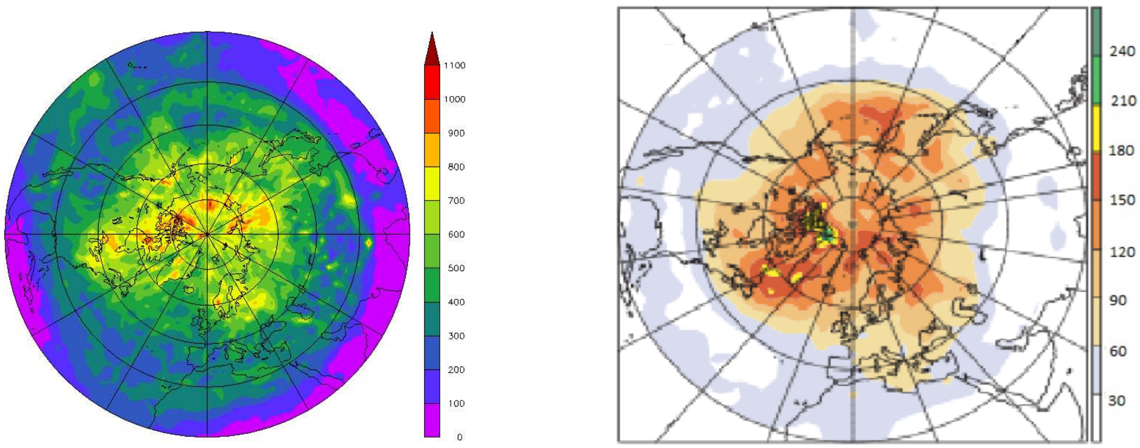

Figure 3.3: Comparison of the upward mass flux (TST) across the 2 PVU iso-surface between our results (left) and the result from Sprenger and Wernli [2003] (right) for the Northern Hemispheric winter (DJF). Both results are in $\mathrm{kgkm^{-2}s^{-1}}$

compare well with those of Sprenger and Wernli [2003] in that the spatial pattern of events across the Northern Hemisphere are similar. It is also necessary to study the magnitudes of the fluxes for both data sets. It is evident when looking at both sets of results that the magnitude of the fluxes do not correspond. Sprenger and Wernli [2003] obtain maxima on the order of 240 kg/km^2/s whereas our results are on the order of 1000 kg/km^2/s. Possible explanations for this discrepancy include the difference in residence threshold times, inter-annual variability, and the difference in resolution size. Possible errors and these differences in the two studies will be further discussed in Chapter 5.

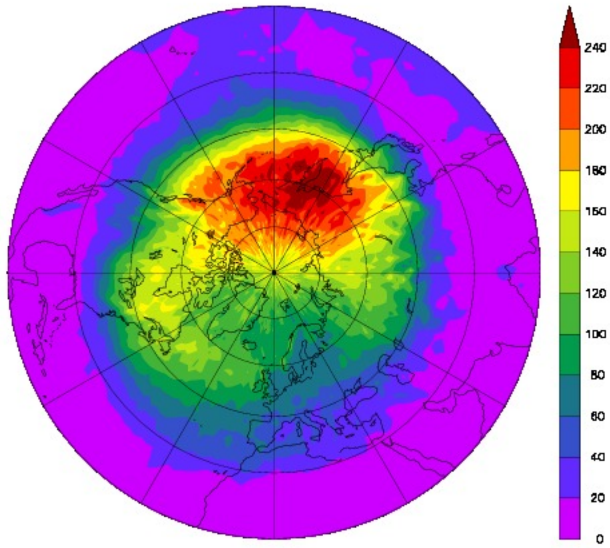

Figure 3.4: Northern Hemisphere mass flux density (kg/s/km^2) downwards across the 380K isentrope for the year September 2010 to August 2011.

There does not exist a study to which we can compare our spatial results of mass flux across the 380K isentrope. However, the dynamics across this surface are well understood and thus the spatial pattern can be inferred. It is well known that the mass flux across the 380K isentrope is dominated by the Brewer-Dobson circulation [Shepherd and McLandress, 2011]. This is a slow overturning circulation consisting of an upward branch in the tropics which is then carried poleward and descends in extra-tropics and polar regions. The strongest downward movement in the Northern Hemisphere occurs between approximately 40^o and 70^oN. Therefore we would expect to see a relatively large flux upwards in the tropics and then downwards in the extra-tropics extending into the polar regions with a maximum between approximately 40^o and 70^oN. In addition the mass flux across the dynamical tropopause is much stronger than across the 380K isentrope, therefore, we would expect the magnitude of the fluxes across the isentrope to be significantly lower.

Figures 3.4 shows the mass flux downwards across the 380K isentrope. The exchange events begin around 40^oN and extend towards the pole. It can

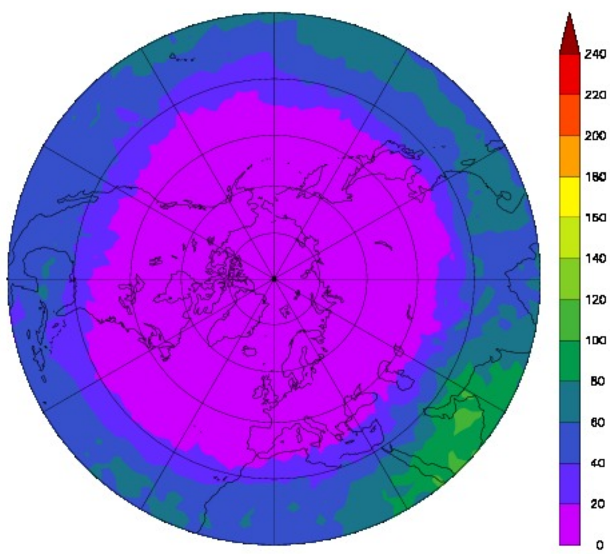

Figure 3.5: Northern Hemisphere mass flux density (kg/s/km^2) upwards across the 380K isentrope for the year September 2010 to August 2011.

also be seen that the maximum occurs between approximately 45^o and 70^oN as expected. Figure 3.5 shows the spatial pattern of upward exchange events across the 380K isentrope. It can be seen that there are significantly fewer events and that they are concentrated equator-ward of 30^oN. As expected, the magnitude of the events are significantly smaller when comparing them with exchanges across the dynamical tropopause. To conclude, although there are no previous papers by with which to spatially compare the mass flux across the 380K isentrope, it can be inferred that our results are consistent with the regions of where the expected downward and upward flux should occur due to the Brewer-Dobson circulation.

Chapter 4

Mass Budget Calculation

4.1 Mass Budget Estimated with the First Forecast Time Window

This STE data set is based on local trajectory calculations and does not necessarily conserve mass. However, if this data set is to be used for the Northern and Southern Hemisphere as well as for long periods of time to study stratosphere troposphere exchange, it needs to estimate properly the transport into and out of the lowermost stratosphere. In order to study the exchange into and out of the LMS, we evaluate the mass budget of the lowermost stratosphere over the Northern Hemisphere using the trajectories from the first forecast time window. These are the trajectories which were initialized at t=00h of the forecast time and are required to cross the boundaries, either the 380K or 2 PVU iso-surfaces, of the lowermost stratosphere within the time window [12h,36h). Since the data set only began in July 2010 and this project studies the one year time frame September 2010 to August 2011, it is unrealistic to expect the net mass flux to vanish. However, because this is the first attempt at using forecast data and the Lagrangian methodology to study STE events on the climatological scale, it is necessary to validate its capability of estimating the net mass flux into the lowermost stratosphere.

4.1.1 Calculating the Mass Budget

The lowermost stratosphere for the Northern Hemisphere is the region bounded on the top by the 380K isentrope and on the bottom by the dynamical tropopause here chosen to be the 2 PVU iso-surface. The 380K isentrope lies around 90 hPa in the tropics and slowly slopes downwards as it moves poleward. The 2 PVU tropopause starts relatively low in altitude at the poles and quickly extends upwards to infinite values as it reaches the equator. Due to the fact that the 2 PVU tropopause has a much steeper slope moving equator-ward, there is an area of intersection around 10-15^o N . Where these two surfaces intersect is the beginning of the lowermost stratosphere and extends from this latitude to the north pole (shaded region in Figure 1.2). The mass flux into the lowermost stratosphere is defined such that a positive value indicates an increase in mass of the LMS and a negative value results in a decrease. More specifically, we defined the mass flux as:

Total mass flux = Mass entering wedge - Mass exiting wedge

where:

Mass entering wedge= Mass crossing 380K downward (380_D) +
Mass crossing 2 PVU upward (PV_U)

and:

Mass exiting wedge = Mass crossing 380K upward (380_U) +
Mass crossing 2 PVU downward (PV_D)

4.1.2 Total Mass Flux for the Northern Hemisphere

Figure 4.1 shows the mass flux into the wedge for a given latitude in units 10^3 kg/km/s. This figure is a zonal representation of mass flux into and out of the wedge shown in Figure 1.2. Figure 4.1 begins at 15^{o}N because this is the general area where the 380K isentrope and dynamical tropopause meet. Any fluxes which cross either of these surfaces equator-ward of 15^{o}N do not enter the wedge shown in Figure 1.2. These mass fluxes do not contribute to the mass budget of the lowermost stratosphere and can be ignored for this thesis.

The mass leaving the wedge, the negative area of the curve, and the mass entering the wedge, the positive area of the graph, should add up to zero in each hemisphere. It is evident from this figure that we have a large annual net mass influx into our wedge. The Northern Hemispheric mass flux under the curve in Figure 4.1 was calculated. This value is 632 x 10^3 kg/s on average. This implies that the mass of lowermost stratosphere on average in the Northern Hemisphere increases by the previous calculated value . From this value we can calculate how long it would take for the mass of the lowermost stratosphere to double. This results in a doubling of the lowermost stratosphere within approximately 60 months over the Northern Hemisphere. This turnover is too fast to be real and cannot be explained through inter-annual variability. There appears to be a systematic error with our calculations of the mass flux. A possible source of error will be investigated in the following sections.

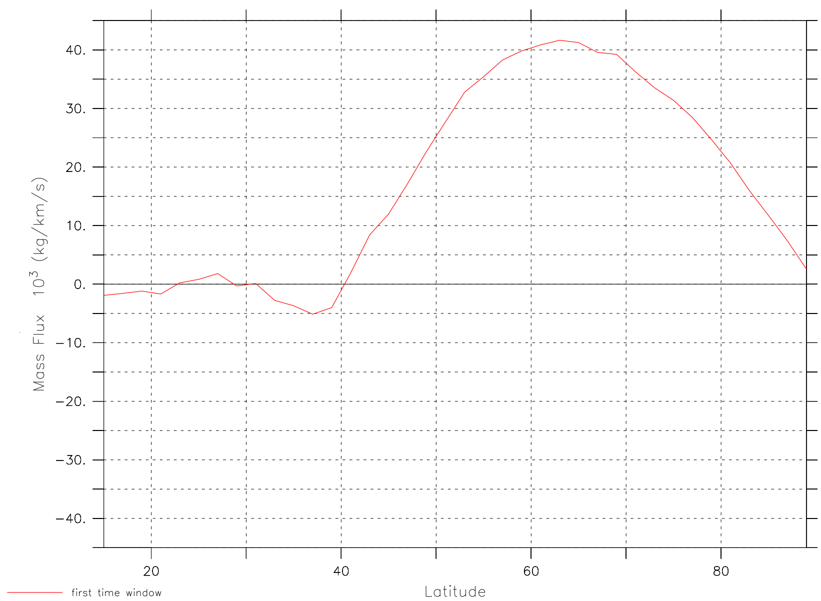

Figure 4.1: Annual mass flux (10^3 kg/km/s) into the LMS from September 2010 to August 2011 for the Northern Hemisphere for all selected trajectories in the first forecast time window per latitude band.

4.2 Mass Budget Estimated with other Forecast Time Windows

We now investigate possible sources of mass flux error using the other forecast time windows. One possibility is that there is a problem with the implementation of our Lagrangian methodology. The relatively good agreement in spatial pattern that our estimated fluxes across the 2 PVU surface showed with Sprenger and Wernli [2003] gave us confidence in this technique. Another possible source of error may have to do with the initialization of the model for each successive forecast. Recall that our fluxes were calculated using Lagrangian trajectories that were initialized at time t=0h and then crossed either the 2 PVU or 380 K surface between t = [12,36). It is possible that model initialization leads to an adjustment process at the beginning of each forecast, and that this leads to a spurious motion of one or both of the surfaces bounding the lowermost stratosphere. In order to investigate this possibility we studied the evolution of the mass flux into the lowermost stratosphere with forecast time.

The previous section used a climatology based on the trajectories which crossed either the 380K surface or the dynamical tropopause that were initialized at t=00h of the forecast time and crossed between the times t=12h and t=36h. However, as described in Chapter 2, the STE data set is also composed of trajectories that were initialized at the times t=24h, t=48h, t=72h, and t=96h of the forecast. Using these, and our previous methodology, we constructed fluxes across the 380K and 2 PVU surfaces for the time windows [36, 60), [60, 84), [84, 108), and [108, 132) hours respectively. This resulted in five yearly climatologies for mass flux into the lowermost stratosphere (refer to Figure 2.2).

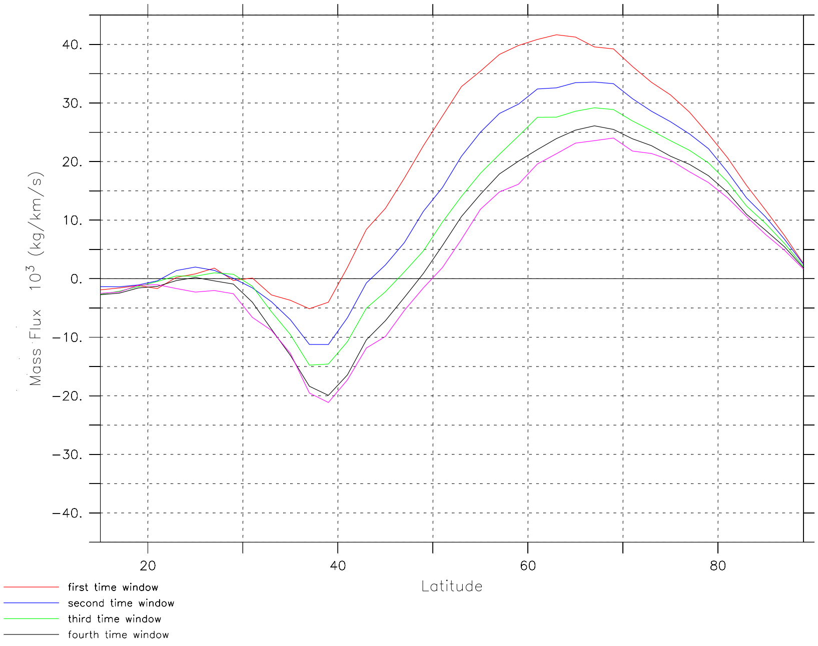

Figure 4.2: Mass flux into the lowermost stratosphere for the Northern Hemisphere from September 2010 to August 2011. The different colours represent the different climatologies based upon forecast time. First forecast time window (red), second forecast time window (blue), third forecast time window (green), fourth forecast time window (black), fifth forecast time window (magenta).

Following the same procedure as in the previous section, the mass flux for each latitude band for the Northern Hemisphere was calculated. Figure 4.2 shows the curves for the mass flux into the wedge for the five different forecast windows from the GEM model. Each curve represents a different forecast time window: the red line (same as Figure 4.1) represents the first one, the blue the second, the green the third, the black the fourth, and the pink the fifth.

The total area under each curve represents the total mass flux into the lowermost stratosphere over the Northern Hemisphere. There are two important points to note from Figure 4.2. First as the forecast time progresses the area under the curve becomes smaller. More specifically in the fifth time window, the positive area between 50°N and 90°N is much smaller also the negative area from 30°N and 50°N is much greater. The result being less total net mass flux into the lowermost stratosphere over the Northern Hemisphere.

The second noteworthy point relates to how the curves are changing as the time window progresses. First, the area under the curves evolves significantly with time. As the forecast time progresses the positive area under the curve diminishes whereas the negative area increases. It can also be seen that these changes in area do not occur linearly. There is the biggest area change between the first and second curve and the smallest change between the fourth and the fifth. This suggests that the curves are converging to a single curve.

It can also be seen in Figure 4.2 that the latitude at which the maximum occurs differs for each curve. The curve from the first forecast window has its maximum mass flux at approximatey 62^oN whereas the final window has its maximum at 69^oN. Conversely, the minima have little, or even no, shift between the first and final forecast time.

Forecast Time	00	24	48	72	96
Net Mass Flux	632.15	448.00	331.17	227.55	169.36
PV_D Mass Flux	1463.79	1595.94	1654.74	1698.99	1720.64
PV_U Mass Flux	1862.28	1847.93	1822.75	1792.13	1776.28
380_D Mass Flux	353.25	315.35	282.62	253.94	232.46
380_U Mass Flux	119.59	119.34	119.52	119.54	118.74

Table 4.1: Different annual mass fluxes (10^3 kg/s) for the Northern Hemisphere dependant on forecast time (h). PV_$D$and PV_U represent the mass flux downwards and upwards across the 2 PVU tropopause respectively. 380_D and 380_U represent the mass flux downwards and upwards across the 380K isentrope, respectively.

Table 4.1 provides the area integrated values for the total amount of net mass flux calculated as a function of the forecast time. The net mass flux decreases by approximately 30% from the first to the second time window. From the second to the third forecast time window there is a slightly smaller decrease of 26%. The percent decrease becomes smaller as the forecast time increases. The final result from the initial to final forecast time window is a total decrease of 73%.

The values from Table 4.1 were plotted on separate graphs such that forecast time was on the x-axis and annual mass flux was on the y-axis. An exponential curve was fit to all the variables in order to further investigate a possible mass flux convergence. The curve has three parameters of the form $y=\beta e^{\gamma x}+\alpha$; where α is the asymptote and represents the value to which the mass flux is converging. The γ parameter controls the slope of the exponential curve, therefore it tells us how quickly the model is converging. The β parameter is calculated such that $\beta+\alpha$ = initial value at t=0. A best fit parameter R^2 was calculated in order to demonstrate how well the data points fit the curve. The main purpose of calculating the determination coefficient, R^2, was to determine whether the points approximate an exponential function as opposed to some other function, such as a polynomial. The values of R^2 can vary between 0 and 1, where 1 represents an exact fit of the data points to an exponential function and 0 indicates no fit.

Figure 4.3 demonstrates visually the convergence of the total net mass flux. The open circles on the graph represent the values from Table 4.1. Overlaid is a best fit exponential curve of the form $y=\beta e^{\gamma x}+\alpha$. In order to suggest if an exponential function best represents the data, R^2 was calculated and found to be 0.9993. This supports the idea that the net annual mass flux does follow an exponential function.

Recall that the most reasonable mass flux curve was that from the fifth time window, while the first time window led to the most unrealistic mass flux. This would suggest that the error is strongest in the earlier time windows. However, in order to be certain that the fifth window is the best estimate, an understanding of what is causing the error is essential.

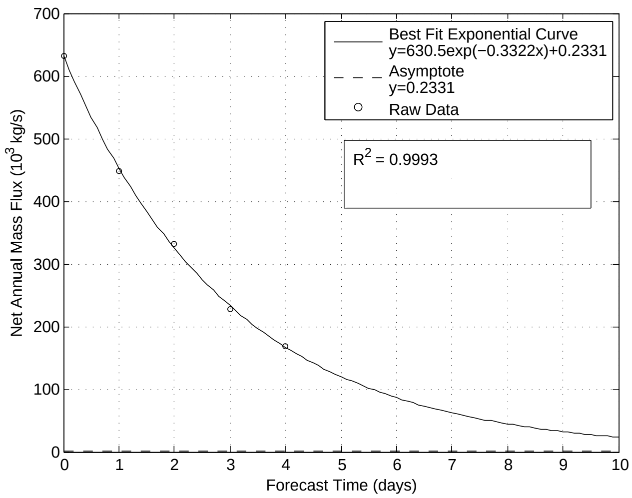

Figure 4.3: Best fit exponential curve for the net mass flux in the lowermost stratosphere. Open circles are the annual fluxes from the trajectory data. The dashed line represents the asymptote.

It was previously shown in Chapter 3 that our method for calculating trajectories across the 2 PVU tropopause was well validated. Furthermore in a study by Bourqui et al. [2012], they show that there is not a general problem with the implementation of the method since their results compared well with observations. Origins of error could therefore be (i) the application of the method to the 380K isentrope and/or (ii) the application of the method to the forecast data. It is well known that when using the variable ω, which is the change in pressure for a given time, as the diagnostic vertical velocity, there will be errors introduced in the calculation of the trajectories [Ploeger et al., 2010]. Since ω uses pressure coordinates, this error will increase with altitude which implies that it may be stronger at the 380K height as opposed to the 2 PVU. Recent studies suggest that this error only becomes significant above 400K [Ploeger et al., 2012]. Additionally, there is no reason why this choice of using ω as a vertical coordinate should depend upon the forecast time.

The second possible error, the application of the method to the forecast data, the previous section suggests that the error maximizes early in the forecast which is close to the initial conditions. It is thus reasonable to suggest that the error arises from the initialization of the GEM model. In other words, a possible source of error is due to the fact that the GEM model is biased but is initialized from unbiased initial conditions. If this were the case, the model would relax to its own state as time progresses from the initial conditions. This would induce erroneous mass fluxes due to the movement of isentropes as well as the 2 PVU tropopause. A further investigation of the GEM model needs to be conducted in order to locate any possible errors.

4.3 A Further Investigation into Possible Errors

In order to analyze a possible bias in the GEM model we first break up the mass flux calculation into its primary parts; that is, the trajectories moving upward and downward across either boundary of the lowermost stratosphere.

There are four basic components in the calculation of the mass budget. We will denote fluxes across the 2 PVU surface as PV_U and PV_D and those crossing the 380K isentrope will be denoted 380_U and 380_D.

4.3.1 380K Isotherm Surface

Figures 4.4 and 4.5 show the zonally integrated mass flux across the 380K isentrope for the Northern Hemisphere in the upwards and downwards directions respectively. The five different lines represent the data calculated from the five different time windows. If there was no bias in the model then when looking at these figures all five of the forecast climatologies would be lying ontop of or near each other. A good example of this is in Figure 4.4 when looking at 380_U. From the initial forecast time until the final forecast time window there is little difference in the mass flux upwards across the 380K surface. This is not the case when looking at the 380_D variable in Figure 4.5. In this case there appears to be a larger mass flux into the wedge at the initial time than at the final forecast time. Furthermore, the curves seem to slowly converge as the forecast time increases. In order to investigate this possibility the total mass flux for both 380_U and 380_D were fitted to an exponential curve which is of the form y=βe$^{\gamma x}$+α, where α is the asymptote and represents the value to which the mass flux is converging.

Figure 4.6 shows a plot of forecast time versus annual mass flux for 380_U. The open circles represent the area under the graphs from the

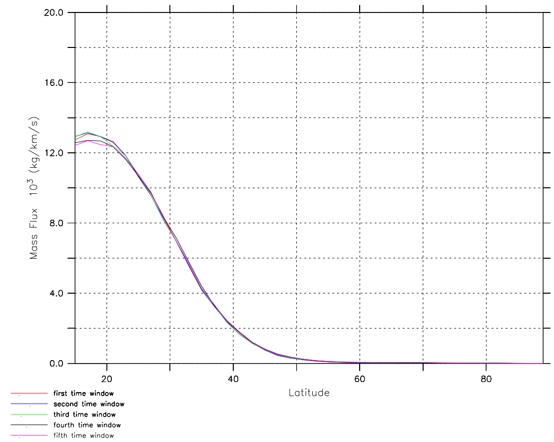

Figure 4.4: Annual mass flux (10^3 kg/km/s) for September 2010 to August 2011 crossing upwards through the 380K isentrope (380_U) in the Northern Hemisphere per latitude band. The different colours represent the different climatologies based upon forecast time. First forecast time window (red), second forecast time window (blue), third forecast time window (green), fourth forecast time window (black), fifth forecast time window (magenta).

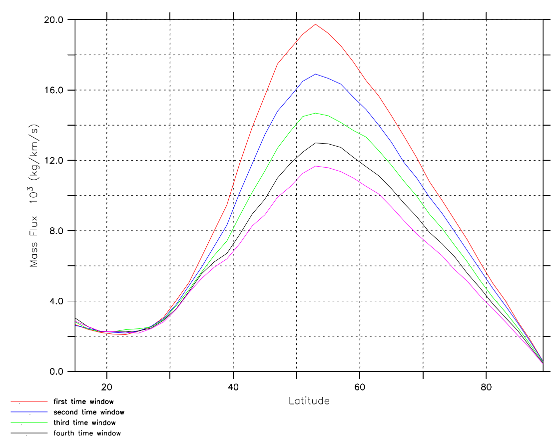

Figure 4.5: Annual mass flux (10^3 kg/km/s) for September 2010 to August 2011 crossing downwards through the 380K isentrope (380_D) in the Northern Hemisphere per latitude band. The different curves represent the different climatologies based upon forecast time. First forecast time window (red), second forecast time window (blue), third forecast time window (green), fourth forecast time window (black), fifth forecast time window (magenta).

previous figure. It can be seen that there is no particular pattern between the forecast time and the mass flux upwards across the 380K surface. This suggests that there is no bias with respect to the mass flux upwards across the 380K isentrope. This is not the case when looking at the mass crossing downwards across the isentrope. Figure 4.7 is a graph of forecast time versus annual mass flux across 380K downwards. The open circles are the calculated values of the mass flux over the Northern Hemisphere and the curve joining them is a best fit exponential. The coefficient of determination, R^2, shows that the curve fits the data points nicely. This suggest that there is a bias when looking at the mass flux downwards across the 380K surface. In order to study this possible bias, we investigated how the 380K isentrope was evolving with time in the GEM model.

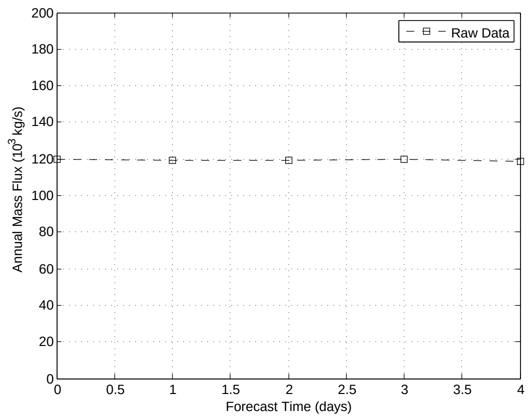

Figure 4.6: Annual mass flux upwards across the 380K isentrope (380_U). Open points represent the annual mass fluxes calculated form the trajectory data. The dashed line connects the five points. (NB this variable does not fit an exponential curve)

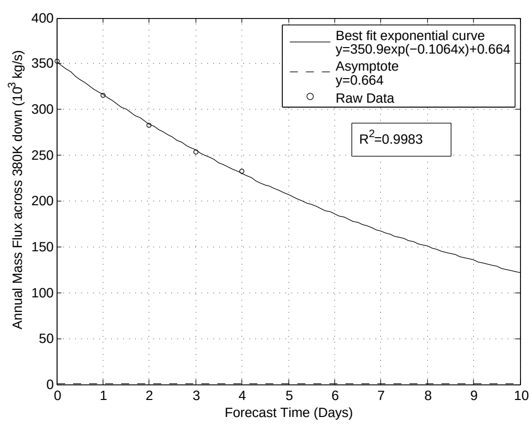

Figure 4.7: Best fit exponential curve for the mass flux downwards across the 380K isentrope (380_D). Open circles are the annual fluxes from the trajectory data. The dashed line represents the asymptote.

Using the GEM forecast, Figure 4.8 shows the pressure difference on the 380K isentrope between the initial and fifth forecast time window with the values in hPa. Since pressure decreases with altitude, a positive value on this figure corresponds to an upward shift in the 380K isentrope with time. In other words, as the forecast time progresses the height of the isentrope increases. In some areas the isentrope height changes by up to 9 hPa. Given that the average height is around 150 hPa in the extra-tropics, such a change in pressure is relatively large.

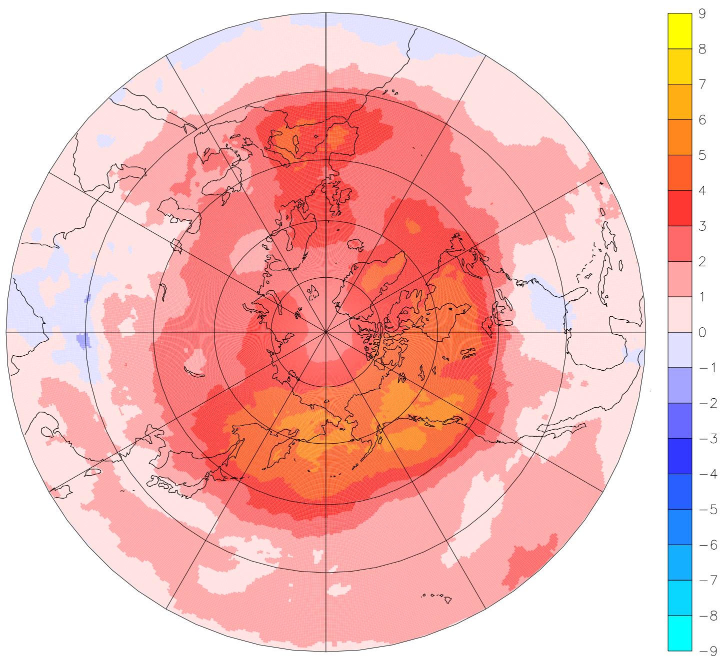

Figure 4.8: The annual difference in height (hPa) of the 380K isentrope from t=00h to t=96h.

One possible explanation is that at the initialization of the forecast, the height of the 380K is too low relative to where the model predicts where it should be started. As time progresses, to counterbalance this there is an influx of mass downwards through the surface in order to push the surface upwards. As the forecast time continues the height of the surface is more accurate thus, less mass flux is required to push the 380K isentrope to higher altitudes. This is consistent with Figure 4.5 in that there is more mass fluxing in initially but as time continues there is progressively less.

4.3.2 2 PVU Iso-surface

Figures 4.9 and 4.10 show the mass flux across the dynamical tropopause (2 PVU surface) per latitude band over the Northern Hemisphere. Each curve represents a different forecast time. The upward mass flux (Fig. 4.9) shows a good general agreement between the different forecast time windows poleward of 65^oN, which suggests that this mass flux is relatively accurately represented in the data. Nevertheless, the spread between the initial and final forecast curve between 20^oN and 60^oN cannot be ignored. The tropopause is located at a higher pressure than the 380K and therefore a mass flux error similar in magnitude to the one across the 380K downwards can be induced by a relatively small vertical displacement.

Figure 4.10 shows the mass flux downward across the 2 PVU surface per latitude band in the Northern Hemisphere. In this case, there is a non-

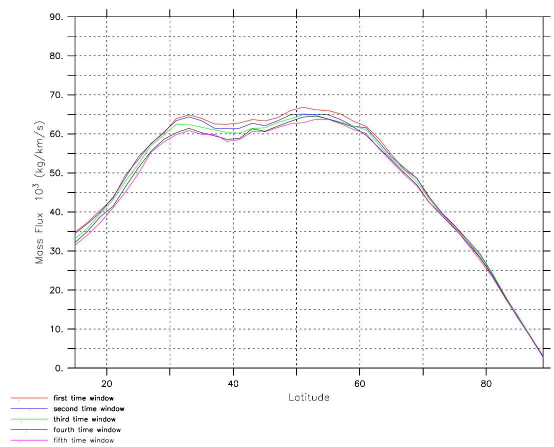

Figure 4.9: Annual mass flux (10^3 kg/km/s for September 2010 to August 2011 crossing upwards through the 2 PVU tropopause (PV_U) in the Northern Hemisphere per latitude band. The different curves represent the different climatologies based upon forecast time. First forecast time window (red), second forecast time window (blue), third forecast time window (green), fourth forecast time window (black), fifth forecast time window (magenta).

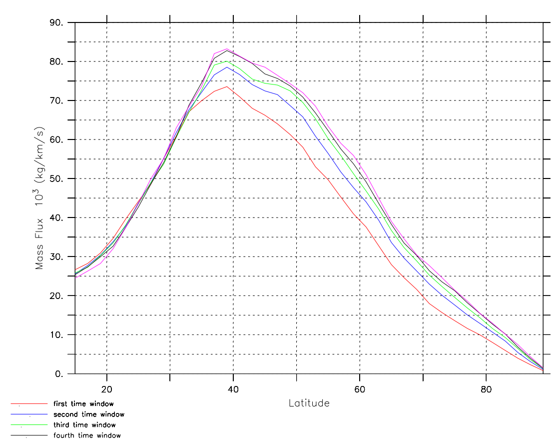

Figure 4.10: Annual mass flux (10^3 kg/kms/s) for September 2010 to August 2011 crossing downwards through the 2 PVU tropopause (PV_D) in the Northern Hemisphere per latitude band. The different curves represent the different climatologies based upon forecast time. First forecast time window (red), second forecast time window (blue), third forecast time window (green), fourth forecast time window (black), fifth forecast time window (magenta).

negligible mass flux difference between the initial and final forecast time poleward of approximately 35^oN. The cross-tropopause mass flux appears to be increasing as the forecast time progresses with decreasing increments. They appear to have converged in the fifth time window. This suggests that there is a convergence of the mass flux across the dynamical tropopause with respect to the forecast time.

An exponential curve was fit to both the PV_D and PV_U variables in order to further investigate a possible mass flux convergence. Figure 4.11 demonstrates the relationship between annual mass flux upwards across the dynamical tropopause and the forecast time. The open circles represent the raw data, the curve is the best fit exponential. It can be seen that there is a slow rate of convergence.

Figure 4.12 shows the relationship between the annual mass flux downwards through the 2 PVU surface and the associated forecast time. Recalling the three other variables, it should be noted that PV_D is the only one which has an increase in annual mass flux with forecast time. Physically, when only looking at this variable, this means that as the forecast time progresses more mass flux is leaving the lowermost stratosphere with time. Looking at Figure 4.12 it can also be seen that this convergence of mass flux occurs quickly. Assuming our exponential curve well represents the data, then extrapolating to the eighth and ninth day we can see that the function has almost approached its asymptote. This implies that by the ninth day the mass flux downwards across the 2 PVU surface has converged to its ultimate value.

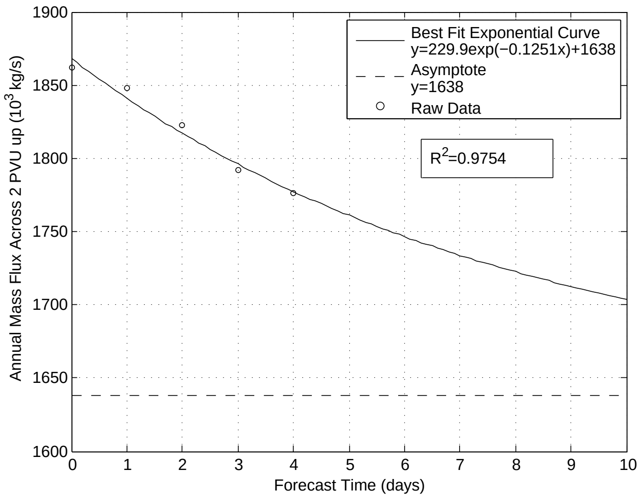

Figure 4.11: Best fit exponential curve for the mass flux upwards across the 2 PVU tropopause (PV_U) per forecast time (days). Open circles are the annual fluxes from the trajectory data. The dashed line represents the asymptote.

Looking at Fig 4.7, 4.11 and 4.12 we can see the relative mass flux errors across the 380K isentrope and 2 PVU surface. The largest errors, that is the difference between annual fluxes during the first and last time window, occur downwards and upwards, respectively across the 2 PVU tropopause followed by that across the 380K isentrope. The asymptotes of each of these exponential curves was assumed to be the value, that if more forecast times were available, the model would converge towards. It was also hypothesized that these values of convergence represent the true state of the mass flux into and out of the LMS. Albeit, this definition may not be agreed upon by all.

Recall that when we studied the transport across the 380K surface there

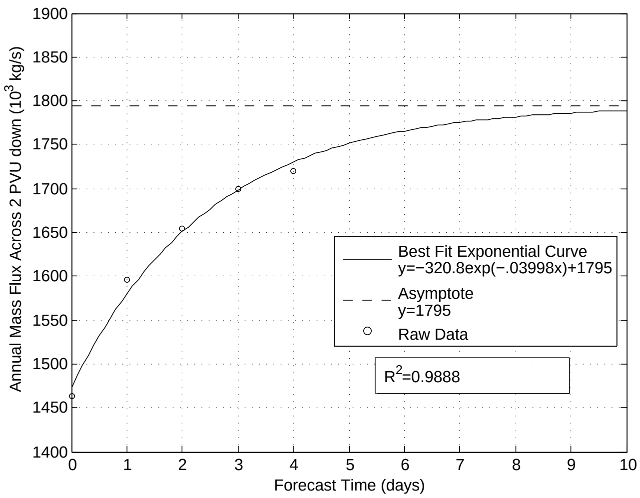

Figure 4.12: Best fit exponential curve for the mass flux downwards across the 2 PVU tropopause (PV_*D*) per forecast time (days). Open circles are the annual fluxes from the trajectory data. The dashed line represents the asymptote.

was an upward transport around the equator and a downward transport in the extra-tropical and polar regions (refer to Figures 3.4 and 3.5). That is transport across the upper boundary of the wedge (the 380K surface) is only dominated by a downward mass flux. This is not the case when studying mass flux across the 2 PVU surface. There exists both upward and downward transport across the tropopause into the wedge. In order to determine which transport is dominating (STT or TST) we calculated the difference of the values from Figures 4.11 and 4.12.

Figure 4.13 demonstrates the net exchange per forecast time. The open circles on the graph are the annual net mass fluxes across the 2 PVU surface where positive values imply the net mass flux is from the troposphere to the stratosphere (upwards). Similarly to the other figures, a best fit exponential curve is overlaid and extrapolated to ten days.

During the first forecast window we see a significant net upward mass flux. As the forecast time progresses, this net transport significantly decreases. We are assuming that the exponential curve well represents our data, and that

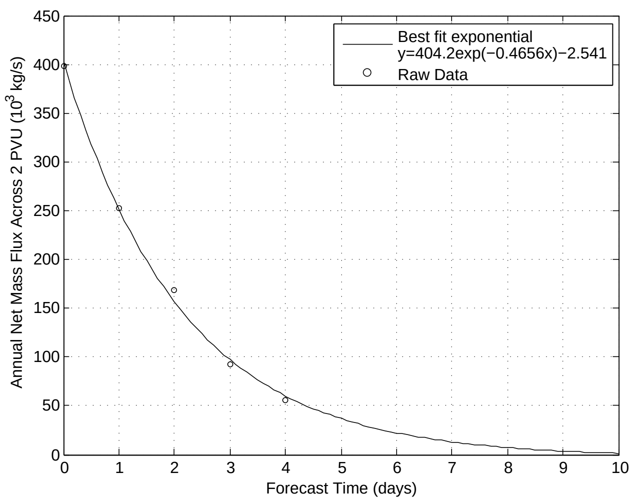

Figure 4.13: Best fit exponential curve for the net mass flux downwards the 2 PVU tsurface per forecast time (days). Open circles are the annual fluxes from the trajectory data.

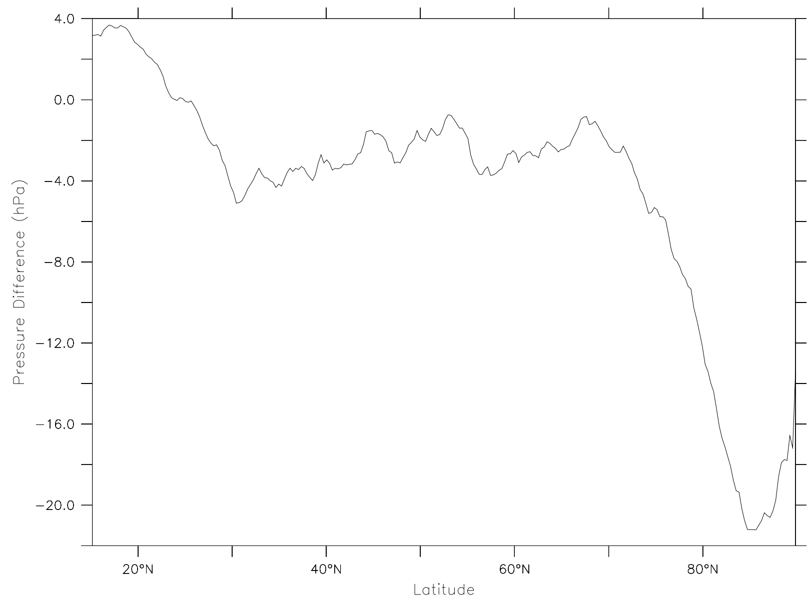

Figure 4.14: Zonally averaged pressure (hPa) of the 2 PVU tropopause at t=00h minus pressure of the tropopause at t=96h over the Northern Hemisphere for the year September 2010 to August 2011

the asymptote is the true value of mass flux across the dynamical tropopause. In this case, the value of the asymptote is -2.541 x 10^3 kg/s which is assumed to be the value of convergence if more forecast times were available. Since the value is negative, it implies a net downward transport across the 2 PVU surface and, thus, out of the wedge. Recall from Figure 3.4 that due to the Brewer-Dobson circulation there is transport downwards across the top layer of the wedge. In order to keep the mass of the LMS constant, then there must be an outflow of mass across the bottom boundary (2 PVU surface). In other words, the downward (STT) mass flux must, in the end, dominate over the upward (TST) mass flux in order for the mass of LMS to remain constant. This is consistent with the value of our asymptote from the net (TST-STT) mass flux across the 2 PVU surface.

Figure 4.13 shows that within the the first five forecast time windows there was a significant upward transport across the 2 PVU surface. There should, therefore, be an associated movement of the 2 PVU surface to compensate for this large influx of mass. Figure 4.14 shows how much the dynamical tropopause has moved between the first and last forecast time. The difference between the pressure of the 2 PVU surface at t=00h and t=96h was calculated. A negative value in the difference in pressure implies the surface has descended. It can be seen that between 15^oN to 27^oN the tropopause moves slightly upward. Poleward of 27^oN there is a descent of the 2 PVU tropopause including a significant downward movement from 70^oN to the pole.

We have shown that the model has a bias in that the 2 PVU surface descends significantly with forecast time. Recall also from Section 4.3.1 that the downward transport across the 380K isentrope was stronger at the initial forecast than the later ones. One question which arises is that of what is causing the height of the tropopause to be so low? Two possible explanations could be as follows: First, the downward transport due to the Brewer-Dobson circulation is too strong in the initial forecast. For the LMS to remain the same mass then we need to have more downward mass flux out of the bottom of the 2 PVU surface. In order to do this, the 2 PVU surface must become more permeable to allow for more transport across the layer. To achieve this, the tropopause must move to higher pressure values. This is consistent with the initial large downward flux through the 380K surface.

The second possibility is that early in the forecast cycle, the permeability of the 2 PVU surface is under represented by the model. In other words, mass entering the wedge from above can not as readily cross the 2 PVU surface below as should be the case. Because of this, the 2 PVU surface descends. As it descends, the surrounding environment has more diabatic activity which acts to compromise the conservation of PV, thus making the surface more permeable. In addition, since density is a multiplying factor in the mass flux equation (refer to Eq. 2.2) at higher pressures there will be an increase in transport. This is consistent with the net fluxes becoming more realistic with forecast time.

4.4 Relationship between Mass Flux and Model Bias

Here we wish to relate the possible biases in the GEM model to the trajectory data. The previous section looked at the difference in pressure heights of the 380K isentrope with respect to the forecast time. An associated mass flux can be calculated from the change in height of this surface. Figure 4.15 shows the amount of mass flux into the wedge associated with the change in pressure of the 380K isentrope from the GEM model data. The total amount of mass flux into the lowermost stratosphere across the 380K isentrope is 1.18 x 10^6 kg/s. Similarly, we can calculate the excess mass flux from our trajectory data by taking the difference of the net downward mass flux between the first and fifth forecast windows (see Figures 4.4 and 4.5). This calculation results in a total mass flux into the wedge of 1.20 x 10^5 kg/s. These numbers are comparable with each other. Together they imply that the bias in the height of the 380K isentrope leads to the transport of trajectories downwards across this surface.

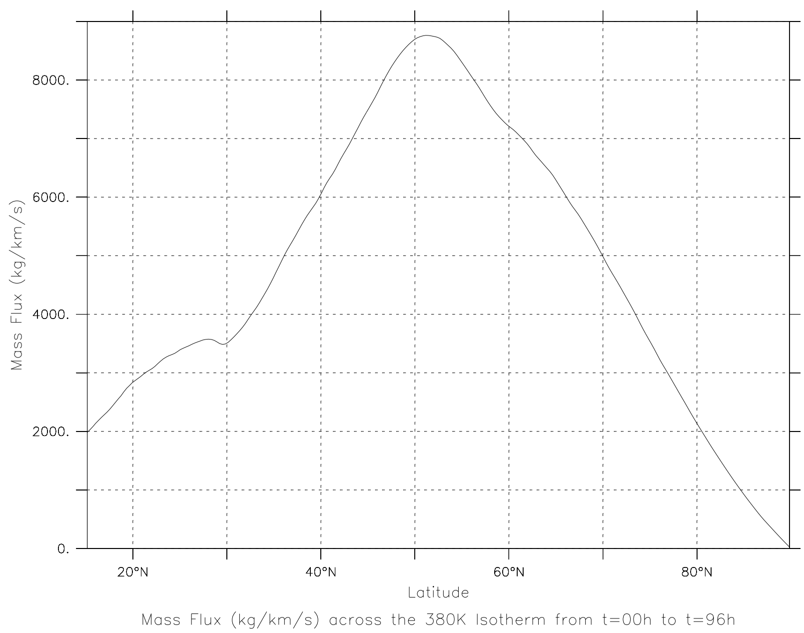

Figure 4.15: Mass flux (kg/km/s) calculated from the difference in pressure levels of the 380K isentrope from t=00h to t=96h from the GEM data

Chapter 5

Discussion and Conclusion

Understanding the locations and rate of air mass exchange between the troposphere and stratosphere has important implications for the lower tropospheric ozone and radiation budget. It has been hypothesized that this cross-tropopause mass flux may increase as a result of climate change [Butchart et al., 2006]. This thesis explored a brand new data set which used a Lagrangian based methodology and the GEM operational forecast model to study transport between the troposphere and stratosphere. Previous methodologies have been used to study the mass exchange between these two layers, however, the Lagrangian based method is advantageous because:

1. It can resolve individual processes.
2. It is capable of considering both intrusion depths and residence times in order to characterize the relative importance of a given exchange event.

When studying stratosphere-to-troposphere exchange (STE) in the extra-tropics an emphasis is placed on the mass flux across the 380K isentrope and the dynamical tropopause. These two surfaces form the upper and lower boundary, respectively, of the Lowermost Stratosphere (LMS) which is the region of interest. The use of 2 PVU as the dynamical tropopause was chosen because it reasonably approximates the thermal tropopause in the extra-tropics [Holton et al., 1995].

The Lagrangian based method was used to calculate the trajectories. This thesis used an adapted version of LAGRANTO [Wernli and Davies, 1997] applied to the output data from the GEM weather forecast model. The motivation of this thesis was to explore this data set such that it can be used in further studies. In order to provide further insight the goals were i) to compare the first one year climatology with previous studies, ii) to analyze the mass budget of the LMS, and iii) to study the relationship between the transport across the 380K isentrope and the dynamical tropopause.

Geographical density maps of upward and downward mass flux across these two surfaces were examined. The flux across the 2 PVU surface was compared with previous results from Sprenger and Wernli [2003]. It was shown, in general, that the two results compared well when looking at the spatial patterns of both upward and downward transport across the dynamical tropopause. However, there were some regions of discrepancy, such as over the Great Lakes and Western Canadian coast (refer to Figure 3.2).

Possible explanations for these discrepancies include inter-annual variability and difference in resolution size. The geographical density maps by Sprenger and Wernli [2003] include fifteen years worth of data whereas our results are only from one year (2010-2011). If the 2010-2011 year had abnormally high or low STE events in these regions we would see this in our results. However, if during one of the years in the Sprenger and Wernli [2003] study they had anomalously high or low amounts of transport, it would be smoothed out by the other fourteen years. Second, Sprenger and Wernli [2003] used a coarser resolution of 2^o x 2^o, compared to our 0.5^o x 0.5^o. This coarser resolution may cause their results to have missed some events because they occurred on smaller horizontal scales, such as thunderstorms. Since our data used a finer resolution, the smaller-scale processes would not have been missed.

After comparing our results and those from Sprenger and Wernli [2003], it was evident that the magnitudes of the exchange events were different approximately by a factor of four. Two possible explanations are minimum threshold residence time and inter-annual variability. The minimum threshold residence time is a criterion which requires that a trajectory remains on either side of the tropopause for a certain amount of time. It has been previously shown that using a minimum threshold residence time, τ^*, of 6h effectively removes spurious oscillations around the tropopause due to numerical noise [James et al., 2003]. In addition, the study by Bourqui [2006] concluded that implementing a τ^* greater than 6h should not affect the spatial pattern. However, reducing the minimum threshold residence time does act to increase the total magnitude of cross-tropopause exchange events. According to the results from Wernli and Bourqui [2002] this will affect the total magnitude of both the upward and downward flux across the dynamical tropopause. Our results used a τ^*=12h whereas Sprenger and Wernli [2003] used 96h. It was shown that this decrease of τ^* may increase the upward and downward exchange fluxes by up to a factor of three. However, this increase in the individual upward and downward components tends to cancel out in the net exchange. Therefore, some of the differences in magnitude between the results can be explained by the difference in threshold residence time.

Another factor which can influence the magnitude of exchange events is inter-annual variability. The magnitude of STE events is not necessarily constant each year. One year may have a large number of events and the next one fewer exchange events. There is less inter-annual variability in Sprenger and Wernli [2003] results because they used fifteen years worth of data. This results in a smoothing of any anomalously high or low exchange years. On the other hand, our results are from one years worth of data. It is very unlikely that inter-annual variability is responsible for the entire difference between the two data sets. However, it might be responsible for a portion of it, and more data is necessary to estimate this problem.

One area of discrepancy between the two data sets occurred over Eastern Asia. This area coincides with approximately the region of the Asian monsoon. It was revealed by Chen [1995] that there is transport between the stratosphere and troposphere due to the Asian monsoon. It was also shown that this is a two-way process, with tracers entering the stratosphere and vice versa [Chen, 1995]. This paper supports our result found in Figure 3.2. However, this area should be studied in more detail.

Unfortunately, there is no previous study to which we can compare our results for the mass flux across the 380K isentrope. Due to our knowledge of the Brewer-Dobson circulation we could infer where to expect both upward and downward transport. We expected to see a large upward flux near the tropics, which corresponds to the upward branch of the Brewer-Dobson circulation. Air begins to descend in the extra-tropics with a maximum occurring around 40^o and 70^oN, therefore we would expect to see a downward flux maximum around these latitudes. Our results for both the downward and upward mass flux across the 380K isentrope were consistent with the associated Brewer-Dobson circulation.

In order to use this data set for further studies, it must be capable of accurately representing the transport into and out of the LMS. Using the one year climatology we studied the total mass flux into the LMS over the Northern Hemisphere. Initially, we used the trajectories from the first forecast time window. When studying the net mass flux per latitude band, we noted a large flux into the wedge in the extra-tropics. At this point we calculated the average total net mass flux into the wedge over an entire year. It was then concluded that this value was too large to be explained through physical processes and that there was a large positive mass flux residual into the wedge which needed to be investigated. Applying the same procedure for the subsequent four forecast times our results showed a decrease in this positive mass flux residual. For each forecast time we calculated the total yearly mass flux into the LMS. We then fit these values to a best fit exponential curve and concluded that the values were tending towards a realistic net mass flux.

In order to investigate the possible errors in the net mass flux calculation, we looked at how the 380K isentrope and dynamical tropopause were evolving with forecast time. For the case of the 380K isentrope, we looked at the difference in pressure on this surface from the first and last forecast window. A difference of up to 9 hPa was observed. It was then hypothesized that the residual was occurring during the initialization of the GEM forecast model. Shortly after the forecast initialization, in order for the model to adjust, there was a large influx of mass downwards across the 380K surface. As the forecast time continued, the model was closer to its own (biased) equilibrium which resulted in less downward transport. Future researchers should be aware of these errors due to model initialization when studying mass flux trends.

When looking at the 2 PVU surface, we saw a large initial flux into the wedge which acted to move the height of the surface to higher pressure values. It was then hypothesized that either the Brewer-Dobson circulation was too strong or the permeability of the 2 PVU surface was under represented in the model. In either case this resulted in the 2 PVU surface moving to higher pressure values. In response, the permeability of the surface increased which explains why there was more downward transport with forecast time. The change in mass flux with forecast time across both boundaries of the LMS supported the hypothesis that the bias was in the GEM model as opposed to the method of trajectory calculation.

This was the first one year climatology of mass flux using this data set. Therefore it has many potential future applications. One useful application which was not studied in this thesis is how the large-scale circulation, due to the Brewer-Dobson circulation, connects with the smaller scale processes. In other words how does the mass flux across the dynamical tropopause respond and react to that across the 380K isentrope or vice-versa? Will an increase in the Brewer-Dobson circulation lead to an increase in activity across the 2 PVU surface? If so, with what time lag would this occur? This data set also allows future researchers to study stratosphere-troposphere transport on a climatological scale in the Southern Hemisphere which has never been done. This could lead to further insight as to specific regions of exchange as well as a mass budget for the Southern Hemisphere.

Bibliography

C. Appenzeller, J.R. Holton, and K. Rosenlof. Seasonal variation of mass transport across the tropopause. *J. Geophys. Res.*, 101:15,071--15,078, 1996.

J.-L. Baray, V. Daniel, G. Ancellet, and B. Legras. Planetary-scale tropopause folds in the southern subtropics. *Geophys. Res. Lett.*, 27:353--356, 2000.

S. Bethan, G. Vaughan, and S.J. Reid. A comparison of ozone and thermal tropopause heights and the impact of tropopause definition on quantifying the ozone content of the troposphere,. *Q. J. R. Meteorol. Soc.*, 122:929--944, 1996.

M. Bourqui. Analysis and quantification of ste: A novel approach. *Swiss Federal Institute of Technology (ETH)*, Ph. D Thesis, 2001.

M. Bourqui. Stratosphere-troposphere exchange from the lagrangian perspective: a case study and method sensitivities. *Atmos. Chem. Phys.*, 6: 2651--2670, 2006.

M. Bourqui and P.-Y. Trépanier. Descent of deep stratospheric intrusions during the ions august 2006 campaign. *J. Geophys. Res.*, 115, 2010. doi: 10.1029/2009JD013183.

M. Bourqui, A. Yamamoto, D. Tarasick, M.D. Moran, L.-P. Beaudoin, I. Beres, J. Davies, A. Elford, W. Hocking, M. Osman, and R. Wilkinson. A new global real-time lagrangian diagnostic system for stratosphere-troposphere exchange: evaluation during a balloon sonde campaign in eastern canada. *Atmos. Chem. Phys. Discuss.*, 12:2661--2679, 2012. doi: 10.5194/acp-12-2661-2012.

A. W. Brewer. Evidence for a world circulation provided by the measurements of helium and water vapor distribution in the stratosphere. *Q. J. R. Meteorol. Soc.*, 75:351--363, 1949.

N. Butchart, A.A. Scaife, M. Bourqui, J. de Grandpre, H.E. Hare, J. Kettleborough, U. Langematz, E. Manzini, F. Sassi, K. Shibata, D. Shindell, and M. Sigmond. Simulations of anthropogenic change in the strength of the brewer-dobson circulation. *Climate Dynamics*, 27:727--741, 2006. doi: 10.1007/s00382-006-0162-4.

P. Chen. Isentropic cross-tropopause mass exchange in the extratropics,. *J. Geophys. Res.*, 100:16,661 -- 16,673, 1995.

W. J. Collins, R.G. Derwent, B. Garnier, C.E. Johnson, M.G. Sanderson, and D.S. Stevenson. Effect of stratosphere-troposphere exchange on the future tropospheric ozone trend. *J. Geophys. Res.*, 108, 2003. doi: 10.1029/2002JD002617.

E. F. Danielsen. Stratospheric-tropospheric exchange based on radioactivity, ozone and potential vorticity. *J. Atmos. Sci.*, 25:502--518, 1968.

G. M. B. Dobson. Origin and distribution of polyatomic molecules in the atmosphere. *Proc. Roy. Soc. Lond.*, A236:187--193, 1956. doi: 10.1098/rspa.1956.0127.

A. Ebel, H. Hass, H.J. Jakobs, M. Laube, M. Memmesheimer, A. Ober-reuter, H. Geiss, and Y.-H. Kuo. Simulation of ozone intrusion caused by a tropopause fold and cut-off low. *Atmos. Environ*, Part A, 25:2131--2144, 1991.

H. Ertel. Ein neuer hydrodynamischer wirbelsatz. *Meteorol. Z.*, 59:277--281, 1942.

A. Gettelman, P. Hoor, L.L. Pan, W.J. Randel, M.I. Hegglin, and T. Birner. The extratropical upper troposphere and lower stratosphere. *Rev. Geophys.*, 49, 2011. doi: 10.1029/2011RG000355.

S. L. Gray. Mechanisms of midlatitude cross-tropopause transport using a potential vorticity budget approach. *J. Geophys. Res.*, 111:D17113, 2006. doi: 10.1029/2005JD006259.

S.L. Gray. A case study of stratosphere to troposphere transport: The role of convective transport and the sensitivity to model resolution. *J. Geophys. Res.*, 108:4590, 2003. doi: 10.1029/2002JD003,317.

J.R. Holton, P.H. Haynes, E.M. McIntyre, A.R. Douglass, R.B. Rood, and L. Pfister. Stratosphere-troposphere exchange. *Rev. Geophys.*, 33:403--439, 1995.

B.J. Hoskins. Towards a pv-theta view of the general circulation. *Tellus, Ser. A*, 43:27--35, 1991.

B.J. Hoskins, M.E. McIntyre, and A.W. Robertson. On the use and significance of isentropic potential vorticity maps. *Q. J. R. Meteorol. Soc.*, 111: 877--946, 1985.

P. James, A. Stohl, C. Forster, S. Eckhardt, P. Seibert, and A. Frank. A 15-year climatology of stratosphere-troposphere exchange with a lagrangian particle dispersion model: 1. methodology and validation. *J. Geophys. Res.*, 108(D12):8519, 2003. doi: 10.1029/2002JD002637.

J. Kowol-Santen, H. Elbern, and A. Ebel. Estimation of cross-tropopause airmass fluxes at midlatitudes: Comparison of different numerical methods and meteorological situations. *American Meteor. Soc.*, 128:4045--4057, 2000.

J.-F. Lamarque, A.O. Langford, and M.H. Proffitt. Cross-tropopause mixing of ozone through gravity wave breaking: Observation and modeling. *J. Geophys. Res.*, 101:22,969--22,976, 1996.

F. Ploeger, P. Konopka, G. Gunther, J.-U. Grooss, and R. Muller. Impact of the vertical velocity scheme on modeling transport in the tropical tropopause layer. *J. Geophys. Res.*, 115:D03301, 2010. doi: 10.1029/2009JD012023.

F. Ploeger, P. Konopka, R. Muller, G. Gunther, J.-U. Grooss, C. Schiller, F. Ravegnani, A. Ulanovski, and M. Riese. Backtrajectory reconstruction of water vapour and ozone in-situ observations in the ttl. *Meteorologische Zeitschrift*, 21:239--244, 2012. doi: 10.1127/0941-2948/2012/0314.

O. Poulida, R.R. Dickerson, and A. Heymsfield. Stratosphere-troposphere exchange in a midlatitude mesoscale convective complex: 1. observations. *J. Geophys. Res.*, 101:6823--6836, 1996.

M.A. Shapiro. Turbulent mixing within tropopause folds as a mechanism for the exchange of chemical constituents between the stratosphere and troposphere. *J. Atmos. Sci.*, 37:994--1004, 1980.

T. Shepherd and C. McLandress. A robust mechanism for strengthening of the brewer-dobson circulation in response to climate change: Critical-layer control of subtropical wave breaking. *J.Atmos. Sci.*, 68:784--797, 2011. doi: 10.1175/2010JAS3608.1.

M. Sprenger and H. Wernli. A northern hemispheric climatology of cross-tropopause exchange for the era 15 time period (1979-1993). 108(D12), 2003.

M. Sprenger, M. Croci Maspoli, and H. Wernli. Tropopause folds and cross-tropopause transport: A global investigation based upon ecmwf analyses for the time period march 2000 to february 2001. *J. Geophys. Res.*, 108(D12): 8518, 2003. doi: 10.1029/2002JD002587.

A. Stohl, P. Bonasoni, P. Cristofanelli, W. Collins, J. Feichter, A. Frank, C. Forster, E. Gerasopoulos, H. Gaggeler, P. James, T. Kentarchos, H. Kromp-Kolb, B. Kruger, C. Land, J. Meloen, A. Papayannis, A. Priller, P. Seibert, M. Sprenger, G.J. Roelofs, H.E. Scheel, C. Schnabel, P. Siegmund, L. Tobler, T. Trickl, H. Wernli, V. Wirth, P. Zanis, and C. Zerefos. Stratosphere-troposphere exchange: A review, and what we have learned from staccato. *J. Geophys. Res*, 108(D12):8516, 2003. doi: 10.1029/2002JD002490.

K. Sudo, M. Takahashi, and H. Akimoto. Future changes in stratosphere-troposphere exchange and their impacts on future tropospheric ozone simulations. *Geophys. Res. Lett.*, 30(24):2256, 2003. doi: 10.1029/2003GL018526.

J. Tremblay and R. Servranckx. Beryllium-7 as a tracer of stratospheric ozone: A case study. *J. Radioanal. Nucl. Chem.*, 172:49--56, 1993.

G. K. Vallis. *Atmospheric and Oceanic Fluid Dynamics*. Cambridge University Press, Cambridge, U.K., 2006.

H. Wernli and M. Bourqui. A lagrangian ‘‘1-year climatology’’ of (deep) cross-tropopause exchange in the extratropical northern hemisphere. *J. Geophys. Res.*, pages 107, D2, 2002. doi: 10.1029/2001JD000812.

H. Wernli and H.C. Davies. A lagrangian-based analysis of extratropical cyclones. i: The method and some applications. *Q.J. R. Meteorol. Soc.*, 123:467--489, 1997.

V. Wirth. Diabatic heating in an axisymmetric cut-off cyclone and related stratosphere-troposphere exchange. *Q. J. R. Meteorol. Soc.*, 121:127--147, 1995b.

V. Wirth and J. Egger. Diagnosing extratropical synoptic-scale stratosphere-troposphere exchange: A case study. *Q. J. R. Meteorol. Soc.*, 125:635--655, 1999.

WMO. Atmospheric ozone 1985. *WMO Global Ozone Res. and Monit. Proj. Rep. 20*, Geneva, 1985.